

Vortex dynamics in 2D antiferromagnets

S. Komineas and N. Papanicolaou
Department of Physics, University of Crete,
and Research Center of Crete,
Heraklion, Greece

Abstract

The dynamics of vortices in a 2D Heisenberg antiferromagnet with an easy-plane anisotropy is studied numerically within the discrete spin model as well as analytically within a continuum approximation based on a suitable extension of the relativistic nonlinear σ model. We find that two like vortices scatter at 90° during a head-on collision, whereas a vortex-antivortex pair is annihilated into spinwave radiation emitted mainly at 90° . When a uniform bias field is applied, vortex dynamics is affected rather profoundly and acquires the characteristic features of the Hall effect of electrodynamics or the Magnus effect of fluid dynamics. In particular, a single vortex is always spontaneously pinned, two like vortices form a rotating bound state, and a vortex-antivortex pair undergoes Kelvin motion. Finally, in the presence of a bias field, vortices are shown to be the prominent topological excitations even for an isotropic antiferromagnet.

I. INTRODUCTION

Topological magnetic solitons have been studied extensively in the case of ferromagnets (FM) and weak ferromagnets (WFM). In both cases a nonvanishing magnetization develops in the ground state, albeit by a different physical mechanism, which allows a detailed experimental investigation by standard techniques [1,2]. In contrast, direct experimental evidence for pure antiferromagnetic (AFM) solitons is limited. Nevertheless, theoretical arguments suggest that static AFM solitons should exist for essentially the same reason as in ordinary ferromagnets, even though their dynamics is significantly different.

The dynamics is now governed by suitable extensions of the relativistic nonlinear σ model [2] instead of the Landau-Lifshitz equation [1]. Therefore dynamical concepts familiar from the theory of FM domain walls and bubbles need to be reanalyzed within the relativistic theory. It is the general purpose of this paper to pursue a study of the dynamics of two-dimensional (2D) AFM solitons that emphasizes the influence of the underlying topological structure. Our starting point is some recent work on AFM and WFM domain walls [3] which revealed that some important issues in the derivation of the associated nonlinear σ model had been mistreated in earlier treatments. We were thus sufficiently motivated to extend the analysis of Refs. [3] to the case of layered or 2D antiferromagnets whose significance has increased in recent years in connection with high- T_c superconductivity.

The present work proceeds by a combination of numerical and analytical methods. Numerical calculations were performed within the standard discrete spin model. However a transparent interpretation of the numerical results could not be achieved without the aid of a continuum approximation at the heart of which lies the relativistic nonlinear σ model. A complete account of the continuum model is given in Sec. II where we discuss, in particular, the relevance of certain parity-breaking contributions that are implicit in spin models involving antiferromagnetic interactions. Numerical and analytical results are then combined in Sec. III to provide a complete description of static AFM vortices.

Subsequent sections are devoted to a detailed study of some special dynamical features due to the underlying topology. For instance, head-on collisions of vortices are examined in Sec. IV and shown to exhibit a characteristic 90° scattering pattern familiar from similar studies of relativistic skyrmions and monopoles [4]. The most surprising element is described in Sec. V where it is shown that an applied uniform magnetic field affects vortex dynamics rather profoundly. A direct link between topology and dynamics is established by means of the conservation laws of linear and angular momentum expressed as moments of a suitable topological vorticity, in analogy with related work for magnetic bubbles in ordinary ferromagnets [5, 6]. Possible phenomenological implications of the derived dynamical picture are further discussed in the concluding Sec. VI. Finally, an Appendix presents some useful virial relations that generalize the well-known scaling theorem of Derrick [7].

II. THE NONLINEAR σ MODEL

We shall study a spin system described by the Hamiltonian

$$W = \sum_{ij} [J \mathbf{S}_{i,j} \cdot (\mathbf{S}_{i+1,j} + \mathbf{S}_{i,j+1}) + \frac{1}{2}g(S_{i,j}^3)^2], \quad (2.1)$$

where the summation extends over all sites of a square lattice, $\mathbf{S}_{i,j}$ is the spin vector at site (i, j) and $S_{i,j}^3$ its third component. Both the exchange constant J and the anisotropy constant g are taken to be positive and hence (2.1) describes a Heisenberg antiferromagnet with an easy-plane single ion anisotropy.

The spin variables are treated as classical vectors with constant magnitude s and satisfy the equation of motion

$$\frac{\partial \mathbf{S}_{i,j}}{\partial t} = \mathbf{S}_{i,j} \times \mathbf{F}_{i,j}, \quad \mathbf{S}_{i,j}^2 = s^2, \quad (2.2)$$

where the effective field \mathbf{F} is determined from the general relation

$$\mathbf{F}_{i,j} = -\frac{\partial W}{\partial \mathbf{S}_{i,j}}, \quad (2.3)$$

or, more explicitly, by

$$\mathbf{F}_{i,j} = -J(\mathbf{S}_{i+1,j} + \mathbf{S}_{i-1,j} + \mathbf{S}_{i,j+1} + \mathbf{S}_{i,j-1}) - gS_{i,j}^3 \mathbf{e}, \quad (2.4)$$

where $\mathbf{e} = (0, 0, 1)$ is a unit vector along the third direction. The exchange contribution in the effective field (2.4) contains fewer than four terms on the perimeter of a finite lattice, the precise number of such terms being equal to the number of nearest neighbors. All dynamical simulations presented in this paper will be based on the above relatively simple set of discrete equations adapted to an open finite lattice.

However, in order to pursue an efficient study of the dynamics, we also consider a continuum approximation which is possible at weak anisotropy,

$$\varepsilon = \sqrt{\frac{g}{J}} \ll 1, \quad (2.5)$$

where soliton structures extend over a large number of sites given roughly by $1/\varepsilon$. The continuum limit is not completely straightforward because of the implicit antiferromagnetic discontinuity as one moves from site to site. It is then important to first identify dynamical variables that may possess a smooth limit as $\varepsilon \rightarrow 0$.

In one dimension continuity is achieved by a simple dimerization process [3]. A square lattice may also be thought of as a collection of dimers, as illustrated in Fig. 1 for a finite lattice cut along the diagonals. The sites of the original square lattice are depicted by two sets of (solid and open) circles which form two intertwining sublattices. This designation is used merely to indicate that the two spins of any given dimer belong to different sublattices. In particular, the ground (Néel) state is such that the

two spins point in opposite directions but are uniform on each sublattice. Because of the easy-plane anisotropy the Néel state is polarized along any direction in the plane perpendicular to the third axis. This azimuthal degeneracy of the ground state will play an important role in the following.

A generic dimer AB (see Fig. 1) is labeled by a pair of indices (α, β) numbered consecutively $(\alpha, \beta = 1, 2, \dots, N)$. In our explicit illustrations N is taken to be even, but this is only a minor technical assumption. Let us denote by $\mathbf{A}_{\alpha, \beta}$ and $\mathbf{B}_{\alpha, \beta}$ the two spins of dimer AB . Eq. (2.2) is then written as a system of two coupled equations,

$$\frac{\partial \mathbf{A}_{\alpha, \beta}}{\partial t} = \mathbf{A}_{\alpha, \beta} \times \mathbf{F}_{\alpha, \beta} \quad \frac{\partial \mathbf{B}_{\alpha, \beta}}{\partial t} = \mathbf{B}_{\alpha, \beta} \times \mathbf{G}_{\alpha, \beta}, \quad (2.6)$$

where the effective fields \mathbf{F} and \mathbf{G} are given by

$$\begin{aligned} \mathbf{F}_{\alpha, \beta} &= -J(\mathbf{B}_{\alpha, \beta} + \mathbf{B}_{\alpha-1, \beta} + \mathbf{B}_{\alpha, \beta-1} + \mathbf{B}_{\alpha-1, \beta-1}) - gA_{\alpha, \beta}^3 \mathbf{e}, \\ \mathbf{G}_{\alpha, \beta} &= -J(\mathbf{A}_{\alpha, \beta} + \mathbf{A}_{\alpha+1, \beta} + \mathbf{A}_{\alpha, \beta+1} + \mathbf{A}_{\alpha+1, \beta+1}) - gB_{\alpha, \beta}^3 \mathbf{e}, \end{aligned} \quad (2.7)$$

for a generic point inside the lattice. The exchange contributions in Eq. (2.7) contain only two terms for each point on the perimeter of the finite lattice of Fig. 1.

As a first step in the derivation of a continuum approximation we introduce the discrete set of variables

$$\eta = \sqrt{2} \varepsilon (\alpha - \alpha_0), \quad \xi = \sqrt{2} \varepsilon (\beta - \beta_0), \quad (2.8)$$

which become continuous in the limit $\varepsilon \rightarrow 0$ and provide a measure of distances along the diagonals of the square lattice. Actual distances are given by $a\eta/\varepsilon$ and $a\xi/\varepsilon$ where a is the physical distance between two neighboring magnetic ions. The lattice constant a will not appear in our theoretical development except when various quantities of interest will have to be translated in physical units. Finally the convenient choice $\alpha_0 = (N+1)/2 = \beta_0$ in Eq. (2.8) sets the origin of the coordinate system at the center of the lattice of Fig. 1.

The main assumption supported by numerical calculations is that the spin variables $\mathbf{A}_{\alpha, \beta}$ and $\mathbf{B}_{\alpha, \beta}$ approach smooth continuum limits $\mathbf{A} = \mathbf{A}(\eta, \xi)$ and $\mathbf{B} = \mathbf{B}(\eta, \xi)$ at weak anisotropy ($\varepsilon \rightarrow 0$). Then we make the substitutions $\mathbf{A}_{\alpha, \beta} \rightarrow \mathbf{A}$ and $\mathbf{B}_{\alpha, \beta} \rightarrow \mathbf{B}$ in Eqs. (2.6)-(2.7) together with the Taylor expansions

$$\begin{aligned} \mathbf{A}_{\alpha \pm 1, \beta} &\rightarrow \mathbf{A} \pm \delta \mathbf{A}_\eta + \frac{1}{2} \delta^2 \mathbf{A}_{\eta\eta}, \\ \mathbf{A}_{\alpha, \beta \pm 1} &\rightarrow \mathbf{A} \pm \delta \mathbf{A}_\xi + \frac{1}{2} \delta^2 \mathbf{A}_{\xi\xi}, \\ \mathbf{A}_{\alpha \pm 1, \beta \pm 1} &\rightarrow \mathbf{A} \pm \delta (\mathbf{A}_\eta + \mathbf{A}_\xi) + \frac{1}{2} \delta^2 (\mathbf{A}_{\eta\eta} + \mathbf{A}_{\xi\xi} + 2\mathbf{A}_{\eta\xi}), \end{aligned} \quad (2.9)$$

and similar expansions for the field \mathbf{B} . Here subscripts denote differentiation with respect to the indicated arguments and

$$\delta = \sqrt{2} \varepsilon \quad (2.10)$$

is used as a temporary notational abbreviation. Eqs. (2.6) are then approximated by

$$\frac{\partial \mathbf{A}}{\partial t} = \mathbf{A} \times \mathbf{F}, \quad \frac{\partial \mathbf{B}}{\partial t} = \mathbf{B} \times \mathbf{G}, \quad (2.11)$$

where

$$\begin{aligned} \mathbf{F} &= -J[4\mathbf{B} - 2\delta(\mathbf{B}_\eta + \mathbf{B}_\xi) + \delta^2(\mathbf{B}_{\eta\eta} + \mathbf{B}_{\xi\xi} + \mathbf{B}_{\eta\xi})] - gA_3\mathbf{e}, \\ \mathbf{G} &= -J[4\mathbf{A} + 2\delta(\mathbf{A}_\eta + \mathbf{A}_\xi) + \delta^2(\mathbf{A}_{\eta\eta} + \mathbf{A}_{\xi\xi} + \mathbf{A}_{\eta\xi})] - gB_3\mathbf{e}, \end{aligned} \quad (2.12)$$

This system of equations is not yet fully consistent because it appears to mix different powers of δ (or ε).

In order to obtain a consistent continuum model we proceed as in the 1D case studied in Ref. [3]. First, we introduce the linear combination of fields

$$\mathbf{m} = \frac{1}{2s}(\mathbf{A} + \mathbf{B}), \quad \mathbf{n} = \frac{1}{2s}(\mathbf{A} - \mathbf{B}), \quad (2.13)$$

which satisfy the constraints

$$\mathbf{m} \cdot \mathbf{n} = 0, \quad \mathbf{m}^2 + \mathbf{n}^2 = 1. \quad (2.14)$$

Second, we define a dimensionless time variable

$$\tau = 2\delta s J t = 2\sqrt{2}\varepsilon s J t. \quad (2.15)$$

An equivalent form of Eqs. (2.11) then reads

$$\begin{aligned} \delta \frac{\partial \mathbf{m}}{\partial \tau} &= -\delta[(\mathbf{m} \times \mathbf{n})_\eta + (\mathbf{m} \times \mathbf{n})_\xi] + \frac{1}{2}\delta^2[\mathbf{n} \times (\mathbf{n}_{\eta\eta} + \mathbf{n}_{\xi\xi} + \mathbf{n}_{\eta\xi}) \\ &\quad - \mathbf{m} \times (\mathbf{m}_{\eta\eta} + \mathbf{m}_{\xi\xi} + \mathbf{m}_{\eta\xi})] - \frac{1}{4}\delta^2[m_3(\mathbf{m} \times \mathbf{e}) + n_3(\mathbf{n} \times \mathbf{e})], \\ \delta \frac{\partial \mathbf{n}}{\partial \tau} &= 4(\mathbf{m} \times \mathbf{n}) + \delta[\mathbf{m} \times (\mathbf{m}_\eta + \mathbf{m}_\xi) - \mathbf{n} \times (\mathbf{n}_\eta + \mathbf{n}_\xi)] \\ &\quad + \frac{1}{2}\delta^2[\mathbf{m} \times (\mathbf{n}_{\eta\eta} + \mathbf{n}_{\xi\xi} + \mathbf{n}_{\eta\xi}) - \mathbf{n} \times (\mathbf{m}_{\eta\eta} + \mathbf{m}_{\xi\xi} + \mathbf{m}_{\eta\xi})] \\ &\quad - \frac{1}{4}\delta^2[m_3(\mathbf{n} \times \mathbf{e}) + n_3(\mathbf{m} \times \mathbf{e})]. \end{aligned} \quad (2.16)$$

A simple inspection of the above equations suggests that consistency is obtained if \mathbf{m} is of order δ . Then the leading approximation of the second equation is

$$\delta \frac{\partial \mathbf{n}}{\partial \tau} = 4(\mathbf{m} \times \mathbf{n}) - \delta[\mathbf{n} \times (\mathbf{n}_\eta + \mathbf{n}_\xi)] \quad (2.17)$$

and the constraints of Eq. (2.14) reduce to

$$\mathbf{m} \cdot \mathbf{n} = 0, \quad \mathbf{n}^2 = 1, \quad (2.18)$$

to within terms of order δ^2 . Therefore taking the cross product of both sides of Eq. (2.17) with \mathbf{n} and using the constraints (2.18) yields

$$\mathbf{m} = \frac{\varepsilon}{2\sqrt{2}}[-(\mathbf{n}_\eta + \mathbf{n}_\xi) + (\mathbf{n} \times \dot{\mathbf{n}})], \quad (2.19)$$

where we have restored the small parameter ε from Eq. (2.10). Finally Eq. (2.19) is inserted in the first of Eqs. (2.16) to give in the limit $\varepsilon \rightarrow 0$ the differential equation

$$\mathbf{n} \times \mathbf{f} = 0, \quad \mathbf{f} = \ddot{\mathbf{n}} - \Delta \mathbf{n} + n_3 \mathbf{e}, \quad (2.20)$$

where Δ is the 2D Laplacian

$$\Delta = \frac{\partial^2}{\partial \eta^2} + \frac{\partial^2}{\partial \xi^2}. \quad (2.21)$$

It is understood that terms of order ε^2 in Eqs. (2.18), (2.20) and order ε^3 in Eq. (2.19) have been neglected.

Therefore the continuum approximation is governed mainly by Eq. (2.20) which is a simple extension of the relativistic nonlinear σ model to include a single ion anisotropy. The corresponding velocity of light is equal to unity thanks to our choice of rationalized space and time variables. In our conventions, the spin magnitude s is a simple multiple of the Planck constant (e.g., $s = \frac{1}{2}\hbar$) and thus carries dimension of action, sJ of frequency and s^2J of energy. The ratio ε of Eq. (2.5) is dimensionless, so is the time variable τ of Eq. (2.15). Also recalling that actual distances are given by $a\eta/\varepsilon$ and $a\xi/\varepsilon$, where a is the lattice constant, we conclude that velocity is measured in units of

$$c = 2\sqrt{2}asJ, \quad (2.22)$$

which coincides with the phase velocity of pure AFM magnons on a square lattice in the long-wavelength limit. More generally, the magnon velocity is given by

$$c = 2asJ\sqrt{\frac{z}{2}}, \quad (2.23)$$

where z is the lattice coordination number. Applied for a square lattice ($z = 4$) Eq. (2.23) reduces to Eq. (2.22), whereas for a chain ($z = 2$) it yields the limiting velocity $c = 2asJ$ of Refs. [3].

Needless to say, a complete description of the original spin model requires knowledge of both fields \mathbf{m} and \mathbf{n} . On the other hand, given a solution $\mathbf{n} = \mathbf{n}(\eta, \xi, \tau)$ of the nonlinear σ model, the field \mathbf{m} may be determined from Eq. (2.19) by simple differentiations and may thus be viewed as an auxiliary field. Yet this apparently straightforward result has been controversial. For instance, the parity-breaking gradient terms in Eq.(2.19) were recently derived within the 1D model and shown to be important for various structural properties of AFM and WFM domain walls [3]. The possible occurrence of such terms had been anticipated on symmetry grounds [8] but this possibility was overlooked in the literature for a long time [9].

One should stress that symmetry arguments do not predict the precise coefficients of the parity-breaking gradient terms in Eq. (2.19) and are generally susceptible to overinterpretation. The danger from this dimerization ambiguity is already present in one dimension and was completely analyzed in Refs. [3]. The situation is only compounded in two dimensions. For example, had we chosen to work with a horizontal instead of the vertical dimerization of Fig. 1, the nonlinear σ model of Eq. (2.20) would not be affected but the gradient terms in Eq. (2.19) would appear as $\mathbf{n}_\eta - \mathbf{n}_\xi$ instead of $\mathbf{n}_\eta + \mathbf{n}_\xi$. This is an indication that the local values of the field \mathbf{m} are sensitive to the mode of dimerization and cannot be literally interpreted as magnetization. However no real mathematical or physical ambiguity appears when the results of a calculation or an experiment are consistently interpreted in reference to a specific mode of dimerization. But an attempt to measure the “magnetization” \mathbf{m} by standard techniques may lead to a fuzzy magnetization curve around any nontrivial soliton structure, unless spin values can be resolved at every site [3].

To press the above picture further we note that dimerization is not the only way to achieve continuity on a square antiferromagnetic lattice. We may also consider the tetrameric configuration illustrated for a finite lattice in Fig. 2. Each tetramer is again labeled by two indices α and β numbered consecutively ($\alpha, \beta = 1, 2, \dots, N$) and spin values are smooth as one moves from corresponding sites of one tetramer to the next. Let us again denote by $\mathbf{A}_{\alpha,\beta}$, $\mathbf{B}_{\alpha,\beta}$, $\mathbf{C}_{\alpha,\beta}$ and $\mathbf{D}_{\alpha,\beta}$ the spins on a generic tetramer $ABCD$ shown in Fig. 2, in terms of which the original equation of motion (2.2) may be written as a system of four coupled equations analogous to Eqs. (2.6). This new system may then be used for the derivation of the continuum approximation by a method similar to the one explained earlier within the dimerization scheme of Fig. 1.

We omit the lengthy algebraic details and simply state the final results. We now use the Cartesian coordinates

$$x = 2\varepsilon(\alpha - \alpha_0), \quad y = 2\varepsilon(\beta - \beta_0), \quad (2.24)$$

which are related to the coordinates η and ξ of Eq. (2.8) by a 45° rotation. Here the origin of the coordinate system is again set at the center of the lattice of Fig. 2 by choosing the arbitrary constants as $\alpha_0 = (N+1)/2 = \beta_0$. Next we assume that the four spins on a tetramer approach smooth continuum limits when $\varepsilon \rightarrow 0$ denoted by \mathbf{A} , \mathbf{B} , \mathbf{C} and \mathbf{D} which are some functions of the spatial coordinates x and y of Eq. (2.24) and the time variable τ of Eq. (2.15). A more convenient set of fields is given by

$$\begin{aligned} \mathbf{m} &= \frac{1}{4s}(\mathbf{A} + \mathbf{B} + \mathbf{C} + \mathbf{D}), & \mathbf{n} &= \frac{1}{4s}(\mathbf{A} - \mathbf{B} + \mathbf{C} - \mathbf{D}), \\ \mathbf{k} &= \frac{1}{4s}(\mathbf{A} + \mathbf{B} - \mathbf{C} - \mathbf{D}), & \mathbf{l} &= \frac{1}{4s}(\mathbf{A} - \mathbf{B} - \mathbf{C} + \mathbf{D}), \end{aligned} \quad (2.25)$$

and satisfy the constraints

$$\begin{aligned} \mathbf{m}^2 + \mathbf{n}^2 + \mathbf{k}^2 + \mathbf{l}^2 &= 1, & \mathbf{m} \cdot \mathbf{k} + \mathbf{n} \cdot \mathbf{l} &= 0, \\ \mathbf{m} \cdot \mathbf{n} + \mathbf{k} \cdot \mathbf{l} &= 0, & \mathbf{m} \cdot \mathbf{l} + \mathbf{n} \cdot \mathbf{k} &= 0. \end{aligned} \quad (2.26)$$

In the strict continuum limit ($\varepsilon \rightarrow 0$) the constraints reduce to

$$\mathbf{m} \cdot \mathbf{n} = \mathbf{k} \cdot \mathbf{n} = \mathbf{l} \cdot \mathbf{n} = 0, \quad \mathbf{n}^2 = 1, \quad (2.27)$$

the fields \mathbf{m} , \mathbf{k} and \mathbf{l} are expressed in terms of \mathbf{n} by

$$\mathbf{m} = \frac{\varepsilon}{2\sqrt{2}}(\mathbf{n} \times \dot{\mathbf{n}}), \quad \mathbf{k} = -\frac{\varepsilon}{2}\mathbf{n}_x, \quad \mathbf{l} = -\frac{\varepsilon}{2}\mathbf{n}_y, \quad (2.28)$$

and \mathbf{n} itself satisfies the differential equation

$$\mathbf{n} \times \mathbf{f} = 0, \quad \mathbf{f} = \ddot{\mathbf{n}} - \Delta \mathbf{n} + n_3 \mathbf{e}, \quad (2.29)$$

where Δ is the 2D Laplacian

$$\Delta = \frac{\partial^2}{\partial x^2} + \frac{\partial^2}{\partial y^2}. \quad (2.30)$$

It is again understood that Eqs. (2.27)-(2.29) are accurate to within terms of order ε^2 .

Although the field \mathbf{n} defined in Eq. (2.25) is not directly related to the field \mathbf{n} of Eq. (2.13), its continuum dynamics is still governed by the nonlinear σ model of Eq. (2.29) which is equivalent to Eq. (2.20). However a clear distinction between the two formulations emerges at the level of the auxiliary fields. We now need three such fields (\mathbf{m} , \mathbf{k} and \mathbf{l}) which are expressed in terms of \mathbf{n} through Eqs. (2.28). These relations reinforce our earlier remarks concerning parity-breaking contributions, namely that they are sensitive to the specific mode of taking the continuum limit. For instance, such contributions are no longer present in the field \mathbf{m} but their effect is accounted for by the new auxiliary fields \mathbf{k} and \mathbf{l} . Once again we must conclude that the local values of the field \mathbf{m} cannot be interpreted literally as magnetization.

The perplexing nature of the auxiliary fields calls for a summary of our main strategy. The continuum model is extensively used to motivate the results discussed in subsequent sections. But all numerical calculations are based on the original discrete equation (2.2). The actual calculations may be performed on an open finite lattice either of the type shown in Fig. 1 or that of Fig. 2. The explicit results may then be employed to construct the fields \mathbf{m} and \mathbf{n} in the former case and the fields \mathbf{m} , \mathbf{n} , \mathbf{k} and \mathbf{l} in the latter. In both cases the validity of the respective continuum models can be verified explicitly for a sufficiently weak anisotropy ($\varepsilon \ll 1$). Nonetheless several apparent paradoxes emerged in the course of our investigation which were all resolved in favor of the formulation presented in this section.

III. STATIC VORTICES

We consider first the problem of finding interesting static solutions within the continuum model. In both formulations developed in the previous section, the basic issue is to determine the field \mathbf{n} from the nonlinear σ model and then proceed with the calculation of the auxiliary fields. Time derivatives vanish in the static limit and one obtains the reduced equations

$$\mathbf{n} \times \mathbf{f} = 0, \quad \mathbf{f} = -\Delta \mathbf{n} + n_3 \mathbf{e}. \quad (3.1)$$

It proves convenient to derive the field \mathbf{f} from a variational argument,

$$\mathbf{f} = \frac{\delta W}{\delta \mathbf{n}}, \quad W = \frac{1}{2} \int [(\partial_\mu \mathbf{n} \cdot \partial_\mu \mathbf{n}) + n_3^2] dx dy, \quad (3.2)$$

where W is the energy functional in the static limit (see Sec. V). The repeated index is summed over two distinct values $\mu = 1$ and 2 corresponding to the two spatial coordinates x and y (or η and ξ). It is also useful to resolve the constraint $\mathbf{n}^2 = 1$ explicitly using, for example, the spherical parametrization

$$n_1 = \sin \Theta \cos \Phi, \quad n_2 = \sin \Theta \sin \Phi, \quad n_3 = \cos \Theta \quad (3.3)$$

in terms of which

$$W = \frac{1}{2} \int [(\partial_\mu \Theta \partial_\mu \Theta) + \sin^2 \Theta (\partial_\mu \Phi \partial_\mu \Phi) + \cos^2 \Theta] dx dy \quad (3.4)$$

and Eqs. (3.1) are equivalent to

$$\frac{\delta W}{\delta \Theta} = 0 = \frac{\delta W}{\delta \Phi}, \quad (3.5)$$

or

$$\Delta \Theta + [1 - (\partial_\mu \Phi \partial_\mu \Phi)] \cos \Theta \sin \Theta = 0, \quad \partial_\mu (\sin^2 \Theta \partial_\mu \Phi) = 0. \quad (3.6)$$

It should be noted that the above static equations are formally identical to those encountered in easy-plane ferromagnets. However the physical interpretation of the field \mathbf{n} is now different and the actual construction of the corresponding AFM solitons on the discrete lattice is effected by the prescriptions of Sec. II.

The simplest solution of Eqs. (3.6) is the ground state configuration $\Theta = \frac{\pi}{2}$ and $\Phi = \phi_0$, where ϕ_0 is an arbitrary constant, for which the energy achieves its absolute minimum ($W = 0$). Such a simple configuration ($n_1 = \cos \phi_0$, $n_2 = \sin \phi_0$, $n_3 = 0$) is consistent with our earlier remark that the ground state is the usual Néel state with spins polarized along any direction in the (12) plane. Nontrivial static solutions are also stationary points of the energy functional W and are subject to limitations imposed by the familiar scaling theorem of Derrick [7]. Applied for the functional (3.4) Derrick's argument yields the virial relation

$$\int \cos^2 \Theta dx dy = 0. \quad (3.7)$$

Therefore one must conclude that nontrivial static solutions with finite energy do not exist.

The above argument does not exclude interesting solutions with infinite energy such as vortices. In fact, the possible existence of vortices is probed by a suitable generalization of the Derrick theorem worked out in the Appendix. Eq. (3.7) is then replaced by

$$\int \cos^2 \Theta dx dy = \pi, \quad (3.8)$$

which not only does not exclude the possibility of vortex solutions but predicts the actual value of their anisotropy energy. However the exchange energy is logarithmically divergent.

To obtain an explicit solution we consider the usual cylindrical coordinates $x = \rho \cos \phi$, $y = \rho \sin \phi$ and make the following ansatz for a vortex located at the origin:

$$\Theta = \theta(\rho), \quad \Phi = \kappa(\phi + \phi_0), \quad (3.9)$$

where $\kappa = \pm 1$ will be referred to as the vortex number and ϕ_0 is an arbitrary constant reflecting the azimuthal symmetry. Then the second equation in (3.6) is automatically satisfied and the first yields

$$\frac{1}{\rho} \frac{\partial}{\partial \rho} \left(\rho \frac{\partial \theta}{\partial \rho} \right) + \left(1 - \frac{1}{\rho^2} \right) \cos \theta \sin \theta = 0. \quad (3.10)$$

The energy (3.4) is accordingly reduced to

$$W = \frac{1}{2} \int_0^\infty \left[\left(\frac{\partial \theta}{\partial \rho} \right)^2 + \frac{\sin^2 \theta}{\rho^2} + \cos^2 \theta \right] (2\pi \rho d\rho) \quad (3.11)$$

and its stationary points are solutions of Eq. (3.10). This equation is consistent with the asymptotic behavior

$$\theta \underset{\rho \rightarrow 0}{\approx} c_1 \rho, \quad \theta \underset{\rho \rightarrow \infty}{\approx} \frac{\pi}{2} - \frac{c_2 e^{-\rho}}{\sqrt{\rho}}, \quad (3.12)$$

where c_1 and c_2 are some constants. The actual solution depicted in Fig.3 was calculated numerically via a relaxation algorithm applied to the restricted energy functional (3.11) taking into account the boundary values (3.12).

Furthermore we note that for every solution θ of Eq. (3.10) a new solution is obtained by the formal replacement $\theta \rightarrow \pi - \theta$. Hence the complete result for the field $\mathbf{n} = (n_1, n_2, n_3)$ reads

$$n_1 = \sin \theta \cos[\kappa(\phi + \phi_0)], \quad n_2 = \sin \theta \sin[\kappa(\phi + \phi_0)], \quad n_3 = \nu \cos \theta, \quad (3.13)$$

where $\theta = \theta(\rho)$ is taken from Fig. 3, while the vortex number κ and the polarity ν are given by

$$\kappa = \pm 1, \quad \nu = \pm 1, \quad (3.14)$$

taken in any combination. In other words, both the vortex ($\kappa = 1$) and the antivortex ($\kappa = -1$) come in two varieties ($\nu = \pm 1$).

The asymptotic behavior (3.12) makes it evident that the centrifugal (second) term in the energy (3.11) diverges logarithmically with the size of the system but the remaining terms are finite. In fact, the numerically calculated anisotropy contribution was found to be in excellent agreement with virial relation (3.8). The weak (logarithmic) divergence of the total energy is not necessarily an obstacle to the production of

vortices in an antiferromagnet. In this respect, one should recall that vortices are easily produced in a rotating cylindrical bucket filled with an ordinary fluid or a superfluid [10]. Furthermore vortex-antivortex pairs have finite energy and should play an important role in thermodynamics.

Keeping with the strategy outlined in the concluding paragraph of Sec. II, we must comment on the manner in which Eq. (3.13) furnishes a vortex on the discrete lattice. The field \mathbf{n} of Eq. (3.13) may be used to calculate the auxiliary field \mathbf{m} of Eq. (2.19) or the fields \mathbf{m}, \mathbf{k} and \mathbf{l} of Eq. (2.28), applied for a static solution ($\dot{\mathbf{n}} = 0$), and thereby determine the original spin configuration on the lattices of Fig. 1 and Fig. 2, respectively. As a check of consistency we have used the resulting spin configuration as initial condition within a fully-dissipative algorithm [3] applied to the complete energy functional (2.1) on a 200×200 lattice. The calculated relaxed state accurately reproduced both the profile of Fig. 3 and the corresponding auxiliary fields for a reasonably small value of the anisotropy constant ($\varepsilon = 0.1$). The spin values on the discrete lattice are partially illustrated in Fig. 4 for both a vortex and an antivortex and exhibit the characteristic antiferromagnetic discontinuity between the two sublattices. Finally we mention that a similar calculation of an AFM vortex can be found in Ref. [11] using an Ising-like instead of a single-ion anisotropy.

Since the vortex solutions described above are present for any finite value of the anisotropy, however weak, it is also of interest to examine the extreme limit of vanishing anisotropy. The static equations (3.1) then reduce to

$$\mathbf{n} \times \Delta \mathbf{n} = 0, \quad \mathbf{n}^2 = 1 \quad (3.15)$$

and are equivalent to the $O(3)$ nonlinear σ model in a 2D Euclidean space. The small parameter ε hidden in the definition of spatial coordinates is no longer related to an anisotropy constant but is an intrinsic scale set by the actual spread of localized solitons. The implied arbitrariness of ε is reflected by the scale invariance of Eq. (3.15) and is already an indication that the corresponding solitons are metastable. Explicit solutions of Eq. (3.15) are the well-known Belavin-Polyakov (BP) instantons [12] viewed here as static solitons in the 2+1 dimensional theory of current interest. They differ from the vortex (3.13) mainly in the asymptotic value of the field \mathbf{n} which is now given by

$$\mathbf{n} \xrightarrow{|\mathbf{x}| \rightarrow \infty} (0, 0, 1) \quad (3.16)$$

and coincides with the ground state configuration of the isotropic antiferromagnet defined up to a global $O(3)$ rotation. Therefore the BP instantons may be called AFM bubbles, by analogy to FM bubbles [1], and are classified by the Pontryagin index or winding number Q which is defined as

$$Q = \frac{1}{4\pi} \int q \, dx dy, \quad q = \frac{1}{2} \varepsilon_{\mu\nu} (\partial_\nu \mathbf{n} \times \partial_\mu \mathbf{n}) \cdot \mathbf{n}, \quad (3.17)$$

where $\varepsilon_{\mu\nu}$ is the 2D antisymmetric tensor, and is integer-valued ($Q = 0, \pm 1, \pm 2, \dots$). The topological density q may also be expressed in terms of the spherical variables as

$$q = \varepsilon_{\mu\nu} \sin \Theta \partial_\nu \Theta \partial_\mu \Phi \quad (3.18)$$

and plays an important role in the dynamical theory of FM bubbles [5,6].

An examination of the asymptotic behavior of Eq. (3.13) suggests that a vortex may be viewed roughly as a half bubble. To push this remark further we calculate the density q for the vortex configuration (3.13),

$$q = \frac{\kappa\nu}{\rho} \frac{\partial \cos \theta}{\partial \rho}, \quad (3.19)$$

where $\theta = \theta(\rho)$ must be taken from Fig. 3. Therefore the winding number calculated from Eq. (3.17) is found to be

$$Q = \frac{1}{2} \kappa\nu [\cos \theta(\infty) - \cos \theta(0)] = -\frac{1}{2} \kappa\nu \quad (3.20)$$

and depends on both the vortex number κ and the polarity ν . This result confirms the vague notion that a vortex is topologically equivalent to a half bubble ($Q = \pm \frac{1}{2}$). However a modified topological charge that is related to the vortex number but not the polarity will arise more naturally in the dynamical context of Sec. V.

IV. HEAD-ON COLLISIONS

Although static AFM solitons are similar to those encountered in ferromagnets, their dynamics is significantly different. For comparison purposes, it is useful to recall at this point the two main dynamical features of FM bubbles: (a) An FM bubble cannot be found in free translational motion; it is always spontaneously pinned or frozen within the ferromagnetic medium. (b) An FM bubble tends to move in a direction perpendicular to an applied magnetic field gradient. For example, a single bubble will undergo a 90° deflection with respect to an externally supplied uniform gradient in the absence of dissipation [5, 6]. In the case of two or more interacting bubbles, a gradient arises intrinsically and leads to a characteristic relative motion similar to the Hall motion of electric charges in a uniform magnetic field or the motion of vortices in a fluid [13].

Property (a) is clearly not the case for AFM bubbles or vortices because of the Lorentz invariance of the underlying nonlinear σ model. Indeed, for any static vortex $\mathbf{n} = \mathbf{n}(\mathbf{x})$ constructed in the preceding section, a vortex propagating freely with an arbitrary speed $v < 1 (= c)$ in, say, the x -direction may be obtained by the elementary Lorentz transformation

$$\mathbf{n}(x, y) \rightarrow \mathbf{n} \left(\frac{x - v\tau}{\sqrt{1 - v^2}}, y \right). \quad (4.1)$$

One may then calculate the corresponding auxiliary fields from Eq. (2.19) or (2.28), taking into account that the dynamical contribution ($\mathbf{n} \times \dot{\mathbf{n}}$) is no longer vanishing, and subsequently construct the spin configuration on the discrete lattice to obtain a rigidly moving AFM vortex.

Similarly, there is no reason to believe that property (b) is sustained for AFM bubbles or vortices. Yet one should expect that topology will continue to play an important role within the relativistic dynamics. A possible manifestation of a topological

effect occurs in the dynamics of two bubbles in a head-on collision. Such a process was studied extensively in the context of the isotropic $O(3)$ nonlinear σ model and shown to exhibit a characteristic 90° scattering pattern [14]. This pattern is certainly unusual from the point of view of ordinary particle dynamics but strongly reminiscent of the 90° deflection of FM bubbles in a field gradient. Of course, the above analogy is superficial but indicates that both the Landau-Lifshitz and the relativistic dynamics are influenced by the underlying topology.

The isotropic nonlinear σ model is special in several ways. In particular, its scale invariance leads to metastable bubbles of arbitrary radius. The radius of each bubble changes during collision and never returns to its initial value [14]. A healthier situation arises in the presence of anisotropy which sets a definite scale for the soliton size. Then individual solitons may be deformed during scattering but will always bounce back to their original shape well after collision. The AFM vortices constructed in Sec. III are examples of 2D solitons with definite scale and their dynamics will be the subject of the remainder of this paper.

The simplest dynamical experiment is to consider the evolution of a pair of two identical vortices which are initially at rest at a relative distance d . Because vortices are extended structures, the above initial configuration is not uniquely defined and generally depends on the details of the physical process that brings the two vortices to their initial positions. However such details may be important for a short transient period but are not expected to significantly influence the global properties of the ensuing motion, especially when the initial distance d is large. Therefore there exists significant freedom in the construction of the initial configuration. The simplest choice is to consider the product ansatz

$$\Omega(x, y) = \Omega_1 \left(x - \frac{d}{2}, y \right) \Omega_1 \left(x + \frac{d}{2}, y \right), \quad (4.2)$$

where Ω is the complex stereographic variable

$$\Omega = \frac{n_1 + in_2}{1 + n_3} = \tan(\Theta/2) e^{i\Phi} \quad (4.3)$$

for the vortex pair and Ω_1 is the corresponding variable for a single vortex. In view of Eq. (3.13) we may write

$$\Omega_1 \left(x \pm \frac{d}{2}, y \right) = \frac{\sin \theta_\pm}{1 + \nu \cos \theta_\pm} e^{i\kappa(\phi_\pm + \phi_0)}, \quad (4.4)$$

where

$$\theta_\pm = \theta(\rho_\pm), \quad \rho_\pm = \sqrt{\left(x \pm \frac{d}{2} \right)^2 + y^2}, \quad \phi_\pm = \arctan \frac{y}{x \pm \frac{d}{2}}, \quad (4.5)$$

and $\theta = \theta(\rho)$ is the profile of Fig. 3. In our simulations we made the specific choices $\kappa = 1$, $\nu = -1$ and $\phi_0 = 0$. The product ansatz (4.2) is then written as

$$\Omega = f(\rho_+) e^{i\phi_+} f(\rho_-) e^{i\phi_-}, \quad f(\rho_\pm) = \cot \frac{\theta_\pm}{2} \quad (4.6)$$

and represents a pair of two identical vortices initially at rest, at a relative distance d on the x -axis.

The remaining steps for a complete specification of the initial configuration on the discrete lattice of, say, Fig. 2 proceed as follows. The field \mathbf{n} is obtained by inverting Eq. (4.3), i.e.,

$$n_1 = \frac{\Omega + \bar{\Omega}}{1 + \bar{\Omega}\Omega}, \quad n_2 = \frac{1}{i} \frac{\Omega - \bar{\Omega}}{1 + \bar{\Omega}\Omega}, \quad n_3 = \frac{1 - \bar{\Omega}\Omega}{1 + \bar{\Omega}\Omega}. \quad (4.7)$$

The auxiliary fields \mathbf{m}, \mathbf{k} and \mathbf{l} are then computed from Eq. (2.28) applied for a static configuration ($\mathbf{n} \times \dot{\mathbf{n}} = 0$). The original spin variables $\mathbf{A}, \mathbf{B}, \mathbf{C}$ and \mathbf{D} on a generic tetramer with coordinates (α, β) are determined from Eq. (2.25) applied for the discrete set of points $x = 2\varepsilon(\alpha - \alpha_0)$ and $y = 2\varepsilon(\beta - \beta_0)$ of Eq. (2.24) with $\alpha, \beta = 1, 2, \dots, N$. The spin configuration is thus specified at every site of the original lattice.

Having determined the initial configuration, the ensuing evolution of the vortex pair was calculated by a numerical solution of the initial-value problem (2.2)-(2.4) using a fourth-order Runge-Kutta algorithm. Typical runs were performed on a 200×200 lattice for a reasonably weak anisotropy $\varepsilon = 0.1$ that leads to a respectable grid $[-10, 10]$ for the dimensionless position variables x and y . The rigidity of our numerical results was frequently checked on larger lattices, up to 400×400 , and stability was improved by reinforcing the constraint $\mathbf{S}_{i,j}^2 = s^2$ at every site of the lattice after every Runge-Kutta step. This numerical trick was borrowed from related simulations in the isotropic nonlinear σ model [14]. On this occasion, it should be emphasized that we do not directly simulate the dynamics of the σ model but rather of the original Heisenberg antiferromagnet. A byproduct of this fact was that various theoretical predictions based on the continuum approximation of Sec. II were verified in detail. In particular, we have been able to illuminate numerous subtle points in connection with the parity-breaking contributions in the auxiliary fields.

The results of the numerical simulation described above revealed no surprises when the two vortices are initially at rest; they begin to drift away from each other along the x -axis apparently in order to minimize their interaction energy. Therefore the calculated behavior is similar to that of two ordinary particles interacting with a repulsive potential. Nevertheless this behavior is already significantly different from the one observed in the case of two interacting FM bubbles which would rotate around each other irrespectively of whether the potential is repulsive or attractive [13].

A more interesting situation arises when the two vortices in Eq. (4.6) are initially Lorentz boosted to velocities \mathbf{v} and $-\mathbf{v}$ and are thus set on a head-on collision course on the x -axis. As expected, the two vortices begin to decelerate thanks to their mutual repulsion. However the future of the process depends crucially on the magnitude of the initial velocity. At low velocities the two vortices approach each other to a minimum distance at which they come to rest and then turn around and move off in opposite directions. When the initial speed exceeds a certain critical value the vortices again decelerate but come sufficiently close to a relative distance where the interaction potential seems to have become attractive. The vortices then begin to accelerate toward each other until they overlap almost completely. More importantly, they subsequently split and reemerge as two separate vortices moving off along the positive and negative

y -direction, thus undergoing a 90° scattering analogous to the one observed in numerical simulations of bubbles in the pure $O(3)$ model [14]. The main difference here is that vortices regain their initial shape except for a flip of their internal phase equal to $\phi_0 = \pm \frac{\pi}{2}$.

The situation described above is illustrated in Fig. 5 which depicts three characteristic snapshots of the collision of two like vortices that start from an initial relative distance $d = 5$ with velocities $\mathbf{v}_1 = (0.65, 0)$ and $\mathbf{v}_2 = (-0.65, 0)$. We have chosen to illustrate only the field \mathbf{n} , through its projection on the (12) plane, and hence the antiferromagnetic discontinuity present in Fig. 4 is not apparent in Fig. 5. However we have actually calculated the spin values on the original lattice and then proceeded with the determination of \mathbf{n} as well as the auxiliary fields. We were thus able to confirm several important details of the formulation presented in Sec. II.

The picture changes drastically in the case of a vortex-antivortex pair initially at rest, at a relative distance d on the x -axis. Such a pair is initially described by the product ansatz

$$\Omega = f(\rho_+)e^{i\phi_+}f(\rho_-)e^{-i\phi_-}, \quad (4.8)$$

where notation is the same as in Eq. (4.6). The subsequent evolution was again studied by a numerical calculation similar to the one described earlier for a pair of two like vortices. The vortex and the antivortex now begin to accelerate toward each other apparently because their interaction potential is attractive. Fig. 6 depicts three characteristic snapshots of the field \mathbf{n} which indicate that the resulting spin configuration shows no sign of a nontrivial topological structure, or that the vortex-antivortex pair is annihilated. Nevertheless a closer examination of the time evolution of the energy density shown in Fig. 7 suggests that the annihilation process is not completely dull. Indeed two distinct lumps of energy are emitted along the positive and negative y -axis which do not correspond to any well defined soliton structures and eventually dissipate into spinwaves. It is interesting that a tendency for a 90° scattering persists even in the present case [14].

To summarize, our calculation of head-on collisions of AFM vortices confirms what appears to be a robust feature of relativistic topological solitons [4, 14]. It is more than clear that a simple theoretical explanation of the observed behavior should be possible to obtain almost independently of the specific dynamical model. However such an explanation has thus far been offered only within the context of some variant or other of collective coordinates. For example, vortices in a Higgs model were discussed along those lines in Ref. [15] and shown to exhibit 90° scattering, at least in the so-called Bogomonly limit. At this point, we do not have a convincing theoretical interpretation of our numerical data for head-on collisions. But the theoretical situation improves significantly in the case of AFM vortices in a uniform magnetic field studied in the following section.

V. VORTICES IN A MAGNETIC FIELD

The effect of an applied uniform magnetic field \mathbf{H} is accounted for by including a Zeeman term in the Hamiltonian (2.1),

$$W \rightarrow W - g_0\mu_0 \sum_{ij} (\mathbf{H} \cdot \mathbf{S}_{i,j}), \quad (5.1)$$

where $g_0 \sim 2$ is the gyromagnetic ratio and $\mu_0 = e/2mc$ is the Bohr magneton divided by the Planck constant. AFM vortices then acquire the general dynamical features of FM bubbles described in the beginning of Sec. IV. Such a radical change of behavior was already speculated in Ref. [16] and is established here by means of unambiguous conservation laws that link the dynamics with the underlying topology. The derived qualitative picture is then confirmed by direct numerical simulations.

The classical ground state is now obtained by assigning a spin value \mathbf{A} on the first sublattice (solid circles) and a value \mathbf{B} on the second (open circles). We further introduce the unit vectors $\mathbf{a} = \mathbf{A}/s$ and $\mathbf{b} = \mathbf{B}/s$ to write for the energy of such a configuration

$$W/s^2J\Lambda = 2(\mathbf{a} \cdot \mathbf{b}) + \frac{1}{4}\varepsilon^2(a_3^2 + b_3^2) - \frac{g_0\mu_0}{2sJ}\mathbf{H} \cdot (\mathbf{a} + \mathbf{b}), \quad (5.2)$$

where ε is the dimensionless anisotropy constant of Eq. (2.5) and Λ is the total number of lattice sites assumed to be large. For a field of strength H applied along the third direction the minimum of (5.2) is achieved by the canted spin configuration of Fig. 8, defined up to an arbitrary azimuthal rotation, where the canting angle is given by

$$\sin \delta = \frac{H}{H_c}, \quad H_c = \frac{(8 + \varepsilon^2)sJ}{g_0\mu_0}, \quad (5.3)$$

for field values in the range $H < H_c$. Above the critical field H_c a transition takes place into a ferromagnetic phase ($\delta = \frac{\pi}{2}$). Actually we shall mostly study the parameter regime where both the anisotropy and the applied field are weak, namely

$$\varepsilon \ll 1, \quad H \ll H_c \approx \frac{8sJ}{g_0\mu_0}, \quad (5.4)$$

which are conditions for the validity of a continuum approximation and are sufficiently nonstringent for practical applications. For future reference, Fig. 8 also displays the two vectors

$$\mathbf{m} = \frac{1}{2}(\mathbf{a} + \mathbf{b}), \quad \mathbf{n} = \frac{1}{2}(\mathbf{a} - \mathbf{b}), \quad (5.5)$$

which may be expressed in terms of the canting angle as

$$\begin{aligned} \mathbf{m} &= (0, 0, \sin \delta) \approx (g_0\mu_0 H/8sJ)(0, 0, 1), \\ \mathbf{n} &= (\cos \delta, 0, 0) \approx (1, 0, 0), \end{aligned} \quad (5.6)$$

where the second steps have been restricted to the parameter regime (5.4). Therefore a nonvanishing magnetization \mathbf{m} develops along the third direction whereas \mathbf{n} is confined in the basal plane.

When the field is turned on, the Néel state is set in a precessional mode that eventually relaxes into the canted state of Fig. 8 thanks to some dissipative process or other that is always present in a realistic antiferromagnet. Throughout this section we shall assume that the field has been turned on sufficiently long to ensure that equilibrium has been achieved in the ground state. The argument is carried out in five steps described in the following five subsections.

A. The continuum model

We now return to the discrete equations (2.6)-(2.7) which we extend according to

$$\mathbf{F}_{\alpha,\beta} \rightarrow \mathbf{F}_{\alpha,\beta} + g_0\mu_0\mathbf{H}, \quad \mathbf{G}_{\alpha,\beta} \rightarrow \mathbf{G}_{\alpha,\beta} + g_0\mu_0\mathbf{H}. \quad (5.7)$$

It is also convenient to introduce the rationalized field [3]

$$\mathbf{h} = h\mathbf{e}, \quad h = \frac{g_0\mu_0 H}{2\sqrt{2}\varepsilon_s J}. \quad (5.8)$$

Eqs. (2.16) are then extended simply by adding a term $\delta(\mathbf{m} \times \mathbf{h})$ to the right-hand side of the first equation and $\delta(\mathbf{n} \times \mathbf{h})$ to the second, where $\delta = \sqrt{2}\varepsilon$. The remaining algebraic details will be omitted here because they are similar to those of Sec. II.

Hence the continuum limit is now governed by the strong inequalities

$$\varepsilon, \varepsilon h \ll 1, \quad (5.9)$$

the fields \mathbf{m} and \mathbf{n} continue to satisfy the constraints

$$\mathbf{m} \cdot \mathbf{n} = 0, \quad \mathbf{n}^2 = 1, \quad (5.10)$$

the auxiliary field \mathbf{m} is given by

$$\mathbf{m} = \frac{\varepsilon}{2\sqrt{2}} [-(\mathbf{n}_\eta + \mathbf{n}_\xi) + (\mathbf{n} \times \dot{\mathbf{n}}) - \mathbf{n} \times (\mathbf{n} \times \mathbf{h})] \quad (5.11)$$

and the field \mathbf{n} satisfies the differential equation

$$\mathbf{n} \times \mathbf{f} = 0, \quad \mathbf{f} = \ddot{\mathbf{n}} - \Delta\mathbf{n} + 2(\mathbf{h} \times \dot{\mathbf{n}}) + (\mathbf{n} \cdot \mathbf{h})\mathbf{h} + n_3\mathbf{e}. \quad (5.12)$$

As a check of consistency one may explicitly verify that the ground state values (5.6) are compatible with the above equations for parameters that satisfy the strong inequalities (5.9). Finally we note that Eq. (5.12) emerges also in connection with the tetramerization scheme of Fig. 2, while the associated auxiliary fields are

$$\begin{aligned} \mathbf{m} &= \frac{\varepsilon}{2\sqrt{2}} [(\mathbf{n} \times \dot{\mathbf{n}}) - \mathbf{n} \times (\mathbf{n} \times \mathbf{h})], \\ \mathbf{k} &= -\frac{\varepsilon}{2}\mathbf{n}_x, \quad \mathbf{l} = -\frac{\varepsilon}{2}\mathbf{n}_y, \end{aligned} \quad (5.13)$$

which should be compared to Eqs. (2.28).

We may thus concentrate on the dynamics of the extended nonlinear σ model (5.12) where the effect of the applied field is twofold; it breaks Lorentz invariance and renormalizes the single ion anisotropy. An efficient study of the dynamics is carried out through a variational principle, namely

$$\mathbf{f} = -\frac{\delta\mathcal{A}}{\delta\mathbf{n}}, \quad (5.14)$$

where \mathcal{A} is the action

$$\mathcal{A} = \int L dx dy d\tau, \quad (5.15)$$

and L is the corresponding Lagrangian density [2]

$$L = \frac{1}{2}[\dot{\mathbf{n}}^2 - (\partial_\mu\mathbf{n} \cdot \partial_\mu\mathbf{n})] + \mathbf{h} \cdot (\mathbf{n} \times \dot{\mathbf{n}}) - \frac{1}{2}[(\mathbf{n} \cdot \mathbf{h})^2 + n_3^2]. \quad (5.16)$$

We further resolve the constraint $\mathbf{n}^2 = 1$ explicitly using, for example, the spherical parametrization (3.3) to write

$$L = \frac{1}{2}[\dot{\Theta}^2 + \sin^2\Theta \dot{\Phi}^2] - \frac{1}{2}[(\partial_\mu\Theta \partial_\mu\Theta) + \sin^2\Theta (\partial_\mu\Phi \partial_\mu\Phi)] \\ + h \sin^2\Theta \dot{\Phi} - \frac{1}{2}(1 + h^2) \cos^2\Theta. \quad (5.17)$$

Hence there exist two pairs of canonical fields given by

$$\psi_1 = \Theta, \quad \pi_1 = \dot{\Theta} \\ \psi_2 = \Phi, \quad \pi_2 = \sin^2\Theta (\dot{\Phi} + h). \quad (5.18)$$

The Hamiltonian is then obtained from

$$W = \int w dx dy, \quad w = \pi_a \dot{\psi}_a - L, \quad (5.19)$$

where the repeated Latin index a is summed over the two distinct values of Eq. (5.18). A more explicit form of the energy density w expressed directly in terms of the field \mathbf{n} reads

$$w = \frac{1}{2}[\dot{\mathbf{n}}^2 + (\partial_\mu\mathbf{n} \cdot \partial_\mu\mathbf{n})] + \frac{1}{2}(1 + h^2)n_3^2, \quad (5.20)$$

where we find no trace of the nonrelativistic term $\mathbf{h} \cdot (\mathbf{n} \times \dot{\mathbf{n}})$ of Eq. (5.16). The energy W is now measured in units of $2\sqrt{2}\epsilon s^2 J$.

Therefore the extended nonlinear σ model (5.12) may be cast in the standard Hamiltonian form

$$\dot{\psi}_a = \frac{\delta W}{\delta\pi_a}, \quad \dot{\pi}_a = -\frac{\delta W}{\delta\psi_a}; \quad a = 1, 2, \quad (5.21)$$

which will be the basis for our subsequent theoretical discussion. For instance, the conserved linear momentum should be given by

$$p_\mu = - \int \pi_a \partial_\mu \psi_a dx dy, \quad (5.22)$$

and the angular momentum by

$$\ell = - \int \pi_a \varepsilon_{\mu\nu} x_\mu \partial_\nu \psi_a dx dy. \quad (5.23)$$

Using the canonical variables of Eq. (5.18) a more explicit form of linear momentum reads

$$p_\mu = - \int (\dot{\Theta} \partial_\mu \Theta + \sin^2 \Theta \dot{\Phi} \partial_\mu \Phi + h \sin^2 \Theta \partial_\mu \Phi) dx dy \quad (5.24)$$

and is in agreement with the expression quoted in Ref. [16]. However the field dependent term in Eq. (5.24) leads to an improper integral for vortex configurations for which $\Theta \sim \frac{\pi}{2}$ and $\Phi \sim \kappa\phi$ at spatial infinity. One would think that this difficulty may be resolved by modifying the momentum density by a total divergence, thus replacing $\sin^2 \Theta \partial_\mu \Phi$ by $(\sin^2 \Theta - 1) \partial_\mu \Phi = -\cos^2 \Theta \partial_\mu \Phi$, which would indeed lead to proper behavior at infinity where $\cos \Theta = 0$. Nevertheless the ambiguity would then be shifted to the origin of the vortex where $\partial_\mu \Phi$ is singular, because Φ is multivalued, while $\Theta = 0$ or π and $\cos \Theta = \pm 1 \neq 0$.

The ambiguities in the linear momentum signal an important link between the dynamics and the underlying topological complexity, in analogy with the situation previously analyzed for FM bubbles [5, 6]. In turn, the relativistic dynamics of AFM vortices studied in earlier sections should be radically altered by the applied field. A complete resolution of the ambiguities is given in subsection C after the ground is prepared in subsection B.

B. Vorticity and the stress tensor

For any 2D field theory that can be brought to the standard Hamiltonian form (5.22) one may define a (scalar) vorticity

$$\gamma = \varepsilon_{\mu\nu} \partial_\mu \pi_a \partial_\nu \psi_a, \quad (5.25)$$

where $\varepsilon_{\mu\nu}$ is the 2D antisymmetric tensor ($\varepsilon_{11} = 0 = \varepsilon_{22}$, $\varepsilon_{12} = 1 = -\varepsilon_{21}$). Terminology is borrowed from fluid dynamics because the quantity γ shares with ordinary vorticity several formal properties. The time derivative of γ is calculated from the Hamilton equations to yield

$$\dot{\gamma} = -\varepsilon_{\mu\nu} \partial_\mu \tau_\nu \quad (5.26)$$

where the vector density

$$\tau_\nu = \frac{\delta W}{\delta \psi_a} \partial_\nu \psi_a + \frac{\delta W}{\delta \pi_a} \partial_\nu \pi_a \quad (5.27)$$

is analogous to the “force density” employed by Thiele [17] in the problem of FM bubbles. It is not difficult to see that τ_ν may be written as a total divergence,

$$\tau_\nu = \partial_\lambda \sigma_{\nu\lambda}, \quad (5.28)$$

where the tensor $\sigma_{\nu\lambda}$ is the stress tensor

$$\sigma_{\nu\lambda} = w\delta_{\nu\lambda} - \frac{\partial w}{\partial(\partial_\lambda\psi_a)}\partial_\nu\psi_a - \frac{\partial w}{\partial(\partial_\lambda\pi_a)}\partial_\nu\pi_a \quad (5.29)$$

calculated for a specific energy density w . Eq. (5.26) then reads

$$\dot{\gamma} = -\varepsilon_{\mu\nu}\partial_\mu\partial_\lambda\sigma_{\nu\lambda} \quad (5.30)$$

and proves to be fundamental for our purposes [5,6].

It should be noted that the preceding discussion makes no distinction between ordinary field theories and those endowed with nontrivial topological structure or related properties. However a clear distinction emerges when we consider the total vorticity

$$\Gamma = \int \gamma \, dxdy = \varepsilon_{\mu\nu} \int \partial_\mu\pi_a\partial_\nu\psi_a \, dxdy, \quad (5.31)$$

which is conserved by virtue of Eq. (5.30) for any field configuration with reasonable behavior at infinity. One may also write

$$\Gamma = \varepsilon_{\mu\nu} \int [\partial_\mu(\pi_a\partial_\nu\psi_a) - \pi_a\partial_\mu\partial_\nu\psi_a] \, dxdy \quad (5.32)$$

to indicate that a vanishing value of the total vorticity is the rule rather than the exception. Indeed, under normal circumstances, the first term in (5.32) is shown to vanish by transforming it into a surface integral at infinity and the second term also vanishes because $\varepsilon_{\mu\nu}\partial_\mu\partial_\nu\psi_a = 0$ for any differentiable function ψ_a . Yet the above conditions may not be met in a field theory with nontrivial topology, a fact closely related to the ambiguities discussed in connection with the linear momentum. In general, the canonical definition of conservation laws is rendered ambiguous when the total vorticity Γ is different from zero.

It is then important to examine more closely the definition of vorticity in the current model. Substitution of the canonically conjugate fields of Eq. (5.18) in Eq. (5.25) and straightforward algebraic manipulation yield the local vorticity

$$\gamma = \varepsilon_{\mu\nu}\partial_\mu(\dot{\mathbf{n}} \cdot \partial_\nu\mathbf{n}) + h\omega, \quad (5.33)$$

where

$$\omega = -\frac{1}{2}[\varepsilon_{\mu\nu} \sin(2\Theta) \partial_\nu(2\Theta)\partial_\mu\Phi]. \quad (5.34)$$

The first term in Eq. (5.33) is an uncomplicated total divergence which leads to a vanishing contribution in the total vorticity Γ of Eq. (5.31). Thus we may write

$$\Gamma = h \int \omega \, dxdy \quad (5.35)$$

and further note that the density ω of Eq. (5.34) resembles the Pontryagin density q of Eq. (3.18) except for an overall factor $-\frac{1}{2}$ and the replacement $\Theta \rightarrow 2\Theta$. The latter suggests considering the three-component vector $\mathbf{N} = (N_1, N_2, N_3)$ with

$$\begin{aligned} N_1 &= 2n_3n_1 = \sin(2\Theta) \cos \Phi, \\ N_2 &= 2n_3n_2 = \sin(2\Theta) \sin \Phi, \\ N_3 &= 2n_3 - 1 = \cos(2\Theta), \end{aligned} \tag{5.36}$$

which is also a unit vector field ($\mathbf{N}^2 = 1$). The density ω may then be written as

$$\omega = -\frac{1}{4}\varepsilon_{\mu\nu}(\partial_\nu\mathbf{N} \times \partial_\mu\mathbf{N}) \cdot \mathbf{N} \tag{5.37}$$

and should be compared to the standard Pontryagin density of Eq. (3.17). Furthermore the field \mathbf{N} satisfies the simple boundary condition

$$\mathbf{N} \xrightarrow{|\mathbf{x}| \rightarrow \infty} (0, 0, -1), \tag{5.38}$$

thanks to the condition $n_3 \rightarrow 0$ satisfied by all relevant field configurations, including the vortex configurations of Sec. III. The net conclusion is that ω is actually the Pontryagin density for the field \mathbf{N} and thus yields an integer-valued total vorticity

$$\Gamma = 2\pi h\kappa, \quad \kappa = 0, \pm 1, \pm 2, \dots, \tag{5.39}$$

where the integer κ will be referred to as the vortex number. Indeed an explicit calculation for a single vortex or antivortex ($\kappa = \pm 1$) discussed in Sec. III confirms Eq. (5.39) for any choice of the polarity ν , in contrast to Eq. (3.20) that depends on both the vortex number and the polarity.

To complete this level of description of the current model we quote an explicit expression for the stress tensor calculated from Eq. (5.29) using as input the energy density (5.20). The final result is

$$\sigma_{\nu\lambda} = w\delta_{\nu\lambda} - (\partial_\nu\mathbf{n} \cdot \partial_\lambda\mathbf{n}), \tag{5.40}$$

where the energy density w may be expressed directly in terms of the field \mathbf{n} through Eq. (5.20).

Finally we mention that the discussion of this subsection possesses a straightforward 3D generalization. For instance, Eq. (5.30) becomes

$$\dot{\gamma}_i = -\varepsilon_{ijk}\partial_j\partial_l\sigma_{kl}, \tag{5.41}$$

where Latin indices i, j, \dots assume three distinct values and ε_{ijk} is the 3D antisymmetric tensor. The stress tensor in Eq. (5.41) is obtained by an obvious 3D extension of Eq. (5.40) and the vorticity $\boldsymbol{\gamma} = (\gamma_1, \gamma_2, \gamma_3)$ is given by

$$\gamma_i = \varepsilon_{ijk}\partial_j\pi_a\partial_k\psi_a = \varepsilon_{ijk}\partial_j(\dot{\mathbf{n}} \cdot \partial_k\mathbf{n}) + h\omega_i, \tag{5.42}$$

where the vector density $\boldsymbol{\omega} = (\omega_1, \omega_2, \omega_3)$ reads

$$\omega_i = -\frac{1}{4}\varepsilon_{ijk}(\partial_k \mathbf{N} \times \partial_j \mathbf{N}) \cdot \mathbf{N} \quad (5.43)$$

and generalizes the scalar Pontryagin density (5.37). Furthermore the vorticity is solenoidal ($\nabla \cdot \boldsymbol{\omega} = 0$) essentially by construction and may thus be derived from a vector potential ($\boldsymbol{\omega} = \nabla \times \mathbf{a}$) which can be used to define a degree of knottedness or helicity of vortex lines,

$$\mathcal{H} \sim \int (\mathbf{a} \cdot \boldsymbol{\omega}) dV, \quad (5.44)$$

by analogy with the Hopf index in ferromagnets [6]. Such an index may prove to be an important issue in the study of 3D antiferromagnets but will not be discussed further in the present paper.

C. Conservation laws

We now return to the 2D theory and consider the derivation of unambiguous conservation laws. Since the main strategy was already explained in the related context of FM bubbles [5,6] our description here will address only the essential points adapted to the present model. The appearance of a double derivative in the right-hand side of the fundamental relation (5.30) suggests that some of the low moments of the local vorticity γ must be conserved. Indeed the linear momentum $\mathbf{p} = (p_1, p_2)$ is given by

$$p_\mu = -\varepsilon_{\mu\nu} I_\nu, \quad I_\nu = \int x_\nu \gamma dx dy, \quad (5.45)$$

and the angular momentum ℓ by

$$\ell = \frac{1}{2} \int \rho^2 \gamma dx dy, \quad (5.46)$$

where $\rho^2 = x^2 + y^2$. The list of conservation laws is completed by the total magnetization μ in the third direction,

$$\mu = \int [\mathbf{e} \cdot (\mathbf{n} \times \dot{\mathbf{n}}) - \hbar n_3^2] dx dy, \quad (5.47)$$

which can be derived directly from the equation of motion.

The preceding identifications are made plausible by inserting the general expression for the vorticity given by Eq. (5.25) in Eqs. (5.45) and (5.46) and by freely performing partial integrations to recover the canonical forms of linear and angular momentum quoted in Eqs. (5.22) and (5.23) which are plagued by the ambiguities discussed in connection with Eq. (5.24). However no such ambiguities occur in Eqs. (5.45) and (5.46) because the local vorticity γ can be obtained directly from the field \mathbf{n} , rather than the angular variables, and is a particularly well defined quantity; see Eqs. (5.35)

and (5.37). In other words, partial integrations should be performed with great care and are often unjustified.

The main point of this theoretical exercise is that the very structure of the conservation laws (5.45)-(5.47) suggests a radical change in the dynamical behavior of vortices in an applied field ($h \neq 0$). The effect of a nonvanishing total vorticity ($\Gamma = 2\pi h\kappa$) becomes apparent by considering the transformation of the moments I_ν of Eq. (5.45) under a translation of coordinates $\mathbf{x} \rightarrow \mathbf{x} + \mathbf{c}$ where $\mathbf{c} = (c_1, c_2)$ is a constant vector,

$$I_\nu \rightarrow I_\nu + \Gamma c_\nu, \quad (5.48)$$

which implies a nontrivial transformation of the linear momentum (5.45) when $\Gamma \neq 0$. This is surely an unusual property, because linear momentum should be expected to remain unchanged under a constant translation of the origin of coordinates, and indicates that the moments I_ν provide a measure of position rather than momentum. Such a fact is made explicit by considering the guiding center vector $\mathbf{R} = (R_1, R_2)$ with coordinates

$$R_\nu = \frac{I_\nu}{\Gamma} = \frac{1}{\Gamma} \int x_\nu \gamma \, dx dy, \quad (5.49)$$

which transforms as $\mathbf{R} \rightarrow \mathbf{R} + \mathbf{c}$ under a constant translation and is thus a measure of position of a spin configuration with $\Gamma \neq 0$. Nevertheless the vector \mathbf{R} is conserved.

A related fact is that the familiar Poisson bracket algebra is significantly affected when $\Gamma \neq 0$. Using the canonical Poisson brackets,

$$\{\pi_a(\mathbf{x}), \psi_b(\mathbf{x}')\} = \delta_{ab} \delta(\mathbf{x} - \mathbf{x}'), \quad (5.50)$$

and the general expression of the local vorticity (5.25) in the definition of the linear momentum (5.45), it is not difficult to establish the relations

$$\{p_1, p_2\} = \Gamma, \quad \{R_1, R_2\} = 1/\Gamma, \quad (5.51)$$

which are strongly reminiscent of the situation in the case of electron motion in a uniform magnetic field, the role of the latter being played here by the total vorticity Γ .

Similarly the angular momentum (5.46) actually provides a measure of the vortex size, a fact made explicit by considering the mean squared radius defined from

$$r^2 = \frac{1}{\Gamma} \int (\mathbf{x} - \mathbf{R})^2 \gamma \, dx dy = \frac{2\ell}{\Gamma} - \mathbf{R}^2, \quad (5.52)$$

which is also conserved. Needless to say, the conservation laws (5.45) and (5.46) resume their ordinary physical significance at vanishing total vorticity ($\Gamma = 0$).

The observed transmutation in the physical significance of the conservation laws of linear and angular momentum implies a radical change in the dynamical behavior of topological solitons. For example, a single AFM vortex or antivortex ($\kappa = \pm 1$) in a uniform magnetic field carries a nonvanishing total vorticity ($\Gamma = \pm 2\pi h$) and thus cannot be found in a free translational motion ($\dot{\mathbf{R}} = 0$). It is always spontaneously pinned or frozen within the antiferromagnetic medium, in contrast to the freely moving

vortices occurring in the relativistic theory at vanishing field. Vortex motion can occur in the presence of other vortices, but the dynamical pattern is also expected to be substantially different from the one obtained at vanishing field in Sec. IV. Specifically, interacting AFM vortices should now behave as ordinary vortices in a fluid or as electric charges in a uniform magnetic field, as demonstrated by direct simulations in subsection D.

The preceding discussion was kept deliberately general in order to emphasize that the emerging qualitative picture is valid in any field theory for which the total vorticity Γ may be different from zero. However it is now useful to express the conservation laws in a more explicit form that takes into account the specific structure of the current model. We thus insert the local vorticity of Eq. (5.33) in Eq. (5.45) to obtain the linear momentum

$$p_\mu = - \int [(\dot{\mathbf{n}} \cdot \partial_\mu \mathbf{n}) + h \varepsilon_{\mu\nu} x_\nu \omega] dx dy, \quad (5.53)$$

where we have performed a partial integration in the first term which is free of all ambiguities. Similarly the angular momentum (5.46) reads

$$\ell = \int [-\varepsilon_{\mu\nu} x_\mu (\dot{\mathbf{n}} \cdot \partial_\nu \mathbf{n}) + \frac{1}{2} h \rho^2 \omega] dx dy. \quad (5.54)$$

As mentioned already, the above conservation laws possess their usual physical significance only at vanishing total vorticity, $\Gamma = 2\pi h \kappa = 0$, which may be achieved when either the applied field h or the vortex number κ vanishes. Otherwise one must consider the guiding center coordinates (5.49) or

$$R_\mu = \frac{1}{2\pi h \kappa} \int [-\varepsilon_{\mu\nu} (\dot{\mathbf{n}} \cdot \partial_\nu \mathbf{n}) + h x_\mu \omega] dx dy \quad (5.55)$$

and the radius r calculated from Eq. (5.52). It should be noted that the preceding conservation laws display some formal similarities to those derived in a model for a superconductor [18,19].

Finally we return briefly to the 3D theory discussed in the concluding paragraph of subsection B and quote the corresponding conservation laws of linear and angular momentum

$$\mathbf{p} = -\frac{1}{2} \int (\mathbf{r} \times \cdot) dV, \quad \mathbf{l} = -\frac{1}{3} \int [\mathbf{r} \times (\mathbf{r} \times \cdot)] dV, \quad (5.56)$$

where $\mathbf{r} = (x, y, z)$, $dV = dx dy dz$ and $\cdot = (\gamma_1, \gamma_2, \gamma_3)$ is the vector vorticity field of Eq. (5.42). It is interesting that (5.56) are formally identical to the conservation laws derived in fluid dynamics, at least for incompressible fluids; see Eqs. (7.2.5) and (7.2.6) of Ref. [20].

D. Interacting vortices

In the presence of a bias field the static vortices of Sec. III adjust to a slightly different shape. It is not difficult to see that the functional form of a static vortex

remains the same as in Eq. (3.13) except that $\theta = \theta(\rho)$ now satisfies the ordinary differential equation

$$\frac{1}{\rho} \frac{\partial}{\partial \rho} \left(\rho \frac{\partial \theta}{\partial \rho} \right) + \left(1 + h^2 - \frac{1}{\rho^2} \right) \cos \theta \sin \theta = 0, \quad (5.57)$$

which differs from Eq. (3.10) only by an additional easy-plane anisotropy with strength equal to h^2 . Consequently Eq. (5.57) reduces to Eq. (3.10) by the simple rescaling $\bar{\rho} = \sqrt{1+h^2}\rho$ and the vortex profile $\theta = \theta(\bar{\rho})$ is again given by Fig. 3 with the replacement $\rho \rightarrow \bar{\rho}$. More importantly, the auxiliary fields (5.11) or (5.13) now contain field dependent terms that are crucial for a correct calculation of the actual spin values on the lattice of Fig. 1 or Fig. 2, respectively.

A pair of like vortices initially at rest is described by the product ansatz (4.2) taking into account the field dependent modifications discussed in the preceding paragraph. The ensuing time evolution of the vortex pair was obtained numerically. Instead of drifting away the two vortices actually begin to rotate around each other, in sharp contrast to the situation described in Sec. IV at vanishing field. In other words, each vortex moves in a direction perpendicular to the applied force, in analogy with the skew deflection of FM bubbles in a field gradient [5,6]. Fig. 9 illustrates the initial configuration together with two characteristic snapshots taken at time intervals such that the pair had rotated roughly by 90° and 180° , respectively. It is interesting to note that a 90° rotation of the pair in real space is always followed by a 90° internal phase shift of each vortex. Fig. 10 depicts the actual trajectories obtained by tracking the points where $|n_3| = 1$. In spite of an apparent initial tendency to drift away, the two vortices eventually orbit around each other, in complete analogy with the 2D motion of two like vortices in an ordinary fluid or two interacting electrons in a uniform magnetic field. The observed departures of the trajectories of Fig. 10 from a circular shape correspond to the well-known Larmor oscillations in the electron problem. These oscillations are expected to be smoothed out in the limit of large relative distance.

The above results are consistent with the qualitative picture suggested by the conservation laws of subsection C. The two-vortex system carries a total vortex number $\kappa = 2$ and thus a nonvanishing total vorticity $\Gamma = 4\pi h$. The guiding center calculated from Eq. (5.55) is initially located at the origin of the coordinate system and remains fixed at all later times. The angular momentum was calculated numerically based on Eq. (5.54) and its time evolution is demonstrated in Fig. 11. Although the two pieces of Eq. (5.54) acquire a nontrivial time dependence, their sum is fairly well conserved. Furthermore the same general picture was obtained by repeating the calculation for a pair of vortices with the same vortex numbers ($\kappa_1 = \kappa_2$) but opposite polarities ($\nu_1 = -\nu_2$). This result is consistent with the fact that the driving issue is the total vorticity $\Gamma = 2\pi h(\kappa_1 + \kappa_2)$ which is independent of the polarities, in contrast to the ordinary winding number Q of Eq. (3.20).

The calculation was further repeated for a vortex-antivortex pair initially described by the product ansatz (4.8) incorporating the appropriate field dependent modifications. Recall that at vanishing field the vortex and the antivortex are attracted toward each other and are eventually annihilated. The situation is drastically different at nonvanishing field. The pair undergoes Kelvin motion roughly along parallel lines that

are perpendicular to the line connecting the vortex and the antivortex. Fig. 12 depicts the initial configuration together with a snapshot taken at a later instance when the pair had moved in formation along the y -axis to a distance approximately equal to the initial relative separation. Fig. 13 demonstrates the actual trajectories (solid lines) obtained by tracking the points where $|n_3| = 1$. Therefore the derived picture is qualitatively identical to the Kelvin motion of a vortex-antivortex pair in an ordinary fluid or the Hall motion of an interacting electron-positron pair in a uniform magnetic field.

Returning to the conservation laws we note that the total vorticity of a vortex-antivortex pair vanishes ($\kappa = \kappa_1 + \kappa_2 = 0$ and hence $\Gamma = 0$). Therefore it is now meaningful to interpret (5.53) as the conserved total linear momentum of the system. A nonvanishing component develops only along the y -axis, i.e., along the direction of motion of the pair, and its conservation is demonstrated in Fig. 14. Again each of the two pieces in Eq. (5.53) exhibits a nontrivial time dependence but their sum is fairly well conserved. On the other hand, it is still meaningful to define individual guiding centers when the pair is widely separated. For example, approximate guiding centers for the vortex and the antivortex may be defined by restricting the integration in Eq. (5.55) to the right and left half plane and setting $\kappa = 1$ and $\kappa = -1$, respectively. The trajectories obtained by tracking the above approximate guiding centers are also shown in Fig. 13 (dashed lines) and are close to two parallel straight lines. The analogy with the motion of an electron-positron pair in a uniform magnetic field is now made more definite. The actual trajectories of the electron and positron undergo Larmor oscillations along the parallel trajectories of their guiding centers, which become increasingly narrower with increasing relative separation. The absence of more than one such oscillation in Fig. 13 is due to our (numerical) inability to follow the motion to a larger distance; see, however, a related calculation of interacting vortices in a charged fluid [19]. Finally we have verified that a vortex-antivortex pair ($\kappa_1 + \kappa_2 = 0$) exhibits Kelvin motion for any choice of relative polarities ($\nu_1 = \nu_2$ or $\nu_1 = -\nu_2$), a fact that reinforces the prominence of the total vorticity Γ in the study of dynamics.

To summarize, a simple comparison of the results of this subsection to those of Sec. IV establishes that the dynamics of AFM vortices is profoundly altered by the applied field, in remarkable analogy with the familiar Hall effect. Nevertheless one should keep in mind that the effect of a bias field on AFM vortices would not have been as drastic without the aid of the underlying nontrivial topological structure.

E. The isotropic antiferromagnet

The special case of an isotropic Heisenberg antiferromagnet is important for both practical and theoretical purposes. The isotropic limit was briefly discussed in the concluding paragraphs of Sec. III in the absence of a bias field. It was then mentioned that the model possesses metastable AFM bubbles, instead of vortices, which are characterized by the standard Pontryagin index (3.17). However, when a bias field is turned on, the picture changes drastically for two reasons. First, the applied field itself supplies an effective easy plane anisotropy that leads to vortices instead of bubbles. Second, the dynamics of vortices departs significantly from the relativistic dynamics of the pure antiferromagnet.

In the remainder of this section we shall briefly describe the necessary modifications of the formalism to accommodate the isotropic model in a uniform magnetic field. Since a single ion anisotropy is no longer available to provide the small parameter ε of Eq. (2.5), such a parameter is now furnished by the applied field which is assumed to be weak:

$$\varepsilon = \frac{g_0 \mu_0 H}{2\sqrt{2} s J} \ll 1. \quad (5.58)$$

The relevant dynamical equations are then obtained from our earlier results by the formal substitution $\mathbf{h} \rightarrow \mathbf{e} = (0, 0, 1)$, or $h \rightarrow 1$, and by omitting the contribution from the single ion anisotropy. Thus the dynamics of the field \mathbf{n} is now governed by the parameter free Lagrangian

$$L = \frac{1}{2}[\dot{\mathbf{n}}^2 - (\partial_\mu \mathbf{n} \cdot \partial_\mu \mathbf{n})] + \mathbf{e} \cdot (\mathbf{n} \times \dot{\mathbf{n}}) - \frac{1}{2}(\mathbf{e} \cdot \mathbf{n})^2, \quad (5.59)$$

which leads to the equation of motion

$$\mathbf{n} \times \mathbf{f} = 0, \quad \mathbf{f} = \ddot{\mathbf{n}} - \Delta \mathbf{n} + 2(\mathbf{e} \times \dot{\mathbf{n}}) + (\mathbf{n} \cdot \mathbf{e})\mathbf{e}. \quad (5.60)$$

The associated auxiliary fields are accordingly given by

$$\mathbf{m} = \frac{\varepsilon}{2\sqrt{2}}[-(\mathbf{n}_\eta + \mathbf{n}_\xi) + (\mathbf{n} \times \dot{\mathbf{n}}) - \mathbf{n} \times (\mathbf{n} \times \mathbf{e})], \quad (5.61)$$

for the lattice of Fig. 1, or

$$\begin{aligned} \mathbf{m} &= \frac{\varepsilon}{2\sqrt{2}}[(\mathbf{n} \times \dot{\mathbf{n}}) - \mathbf{n} \times (\mathbf{n} \times \mathbf{e})], \\ \mathbf{k} &= -\frac{\varepsilon}{2}\mathbf{n}_x, \quad \mathbf{l} = -\frac{\varepsilon}{2}\mathbf{n}_y, \end{aligned} \quad (5.62)$$

for the lattice of Fig. 2. Finally we must set $h = 1$ throughout our discussion of conservation laws.

Therefore the corresponding physical picture can be readily inferred without further calculation. Static vortices are formally identical to those of Sec. III but their dynamics is similar to the nonrelativistic dynamics of the current Sec. V, for any finite value of the applied field. In other words, to the extent that topological solitons are relevant for the physics of an isotropic antiferromagnet, the dynamical picture is changed significantly even by a very weak bias field.

VI. CONCLUDING REMARKS

The emphasis in the main text was placed on elementary processes involving only two AFM vortices, in order to clearly illustrate an important link between topology and dynamics. However further progress in that direction hinges upon the actual production of isolated vortices. Although there exist several examples of realistic

antiferromagnets that are effectively two-dimensional, including the parent compounds of high- T_c superconductors, there seems to be no direct experimental evidence for isolated AFM vortices or bubbles. This situation is in marked contrast to the observed abundance of ferromagnetic bubbles, vortices in superfluid helium, or Abrikosov vortices in superconductors, and may change in the future.

The qualitative picture derived from elementary processes must also influence the thermodynamics of 2D antiferromagnets. Work in that direction was already presented in Refs. [21, 22] for both Ising-like and single-ion anisotropy, while the effect of an applied field was considered in Ref. [16]. It is clear that much remains to be done in connection with the anticipated Berezinskii-Kosterlitz-Thouless (BKT) phase transition which relies on the dynamics of a gas of interacting vortices and antivortices. Suffice it to say that the dynamics of vortex-antivortex pairs studied in Sec. IV is radically modified by an applied magnetic field discussed in Sec. V. The BKT theory may have to be reformulated in a way that clearly reflects the fundamental change of behavior in the elementary vortex processes when a field is turned on.

Perhaps the clearest manifestation of the effect of an applied field will emerge in the thermodynamics of an isotropic antiferromagnet. Topological solitons at vanishing field are metastable AFM bubbles that obey relativistic dynamics. However the smallest external field will trigger Hall dynamics for AFM vortices which become the relevant topological excitations. Again a successful BKT theory must reflect this abrupt transition in the limit of vanishing field.

Our discussion is concluded with some comments on a variation of the main theme that has not been treated in this paper. An easy-axis anisotropy ($g < 0$) would lead to a ground (Néel) state that is polarized along the easy axis. Therefore topological solitons must then satisfy the simple boundary condition (3.16) and would be AFM bubbles classified by the standard Pontryagin index (3.17). However an application of the Derrick theorem either in its original form or its extended version discussed in the Appendix leads to the conclusion that such solitons do not exist either with finite or infinite energy. This is a notable difference from FM bubbles that occur in easy-axis ferromagnets. The latter are stabilized by a combination of the effects of the long-range magnetostatic field created in a ferromagnetic film and of an applied bias field [6].

Nevertheless, when an easy-axis antiferromagnet is immersed in a uniform magnetic field pointing along the symmetry axis, an effective easy-plane anisotropy is produced that competes with the easy-axis anisotropy. And, when the field exceeds a certain critical value, a spin-flop transition takes place from the Néel state polarized in the third direction to a canted state of the type shown in Fig. 8 which exhibits azimuthal degeneracy. Consequently AFM vortices reappear above the critical value of the applied field and their dynamical properties are very similar to those discussed in Sec. V.

ACKNOWLEDGMENTS

We are grateful to W.J. Zakrzewski for his hospitality at Durham and for discussion of some of the issues presented in this paper. The work was supported in part by a grant from the EEC(CHRX-CT93-0332) and by a bilateral Greek-Slovak research program.

APPENDIX: VIRIAL THEOREMS

We derive a slight generalization of the Derrick theorem [7] that is not based on the assumption of finite soliton energy. The method is an elementary extension of our earlier work on magnetic bubbles [6]. We consider only static solutions for which the stress tensor (5.40) in the absence of an external field reduces to

$$\begin{aligned}\sigma_{\nu\lambda} &= w\delta_{\nu\lambda} - [(\partial_\nu\Theta\partial_\lambda\Theta) + \sin^2\Theta(\partial_\nu\Phi\partial_\lambda\Phi)], \\ w &= \frac{1}{2}[(\partial_\mu\Theta\partial_\mu\Theta) + \sin^2\Theta(\partial_\mu\Phi\partial_\mu\Phi) + \cos^2\Theta],\end{aligned}\tag{A.1}$$

and satisfies the continuity equation

$$\partial_\lambda\sigma_{\nu\lambda} = 0,\tag{A.2}$$

on account of the static Hamilton equations (3.5).

A series of virial relations may now be derived by taking suitable moments of (A.2), the simplest possibility being

$$\int_A x_\nu\partial_\lambda\sigma_{\mu\lambda}dxdy = 0,\tag{A.3}$$

where the integration extends over some finite region A in the 2D plane. An application of the divergence theorem yields

$$\int_A \sigma_{\mu\nu}dxdy = \oint_C x_\nu\sigma_{\mu\lambda}ds_\lambda,\tag{A.4}$$

where the integral in the right-hand side is taken over the closed curve C surrounding the area A; by convention the line-element vector (ds_1, ds_2) is perpendicular to the curve. On the assumption that all fields approach asymptotic values such that the volume integrals in the left-hand side are finite and the surface integrals in the right-hand side vanish, when the integration extends to infinity, one obtains the virial relations

$$\int \sigma_{\mu\nu}dxdy = 0,\tag{A.5}$$

where $\mu, \nu = 1$ or 2 are taken in any combination. It is not difficult to see that relations (A.5) may also be obtained by a Derrick-like argument where coordinates are rescaled according to $x \rightarrow \lambda_{11}x + \lambda_{12}y$, $y \rightarrow \lambda_{21}x + \lambda_{22}y$ and we further demand that the resulting total energy be stationary at $\lambda_{11} = 1 = \lambda_{22}$ and $\lambda_{12} = 0 = \lambda_{21}$. In fact, the original scaling relation of Derrick may be recovered by taking the trace of Eq. (A.5):

$$\int tr\sigma dxdy = 0.\tag{A.6}$$

Substitution in Eq. (A.6) of the explicit stress tensor (A.1) reproduces Eq. (3.7) which contradicts the existence of solitons with finite energy, the latter requirement being

implicit in the transition from Eq. (A.4) to Eq. (A.5) as well as in the original argument of Derrick [7].

In order to probe the existence of interesting static solutions with infinite energy, we return to Eq. (A.4) and take the limit $A \rightarrow \infty$ more carefully. For definiteness let us restrict our attention to the axially symmetric configuration of Eq. (3.9), i.e., $\Theta = \theta(\rho)$ and $\Phi = \kappa(\phi + \phi_0)$ with $\kappa = \pm 1$, which is inserted in the stress tensor (A.1) to yield the reduced elements

$$\begin{aligned}\sigma_{11} &= -U \cos(2\phi) + V, & \sigma_{22} &= U \cos(2\phi) + V, \\ \sigma_{12} &= -U \sin(2\phi) = \sigma_{21},\end{aligned}\tag{A.7}$$

where the functions

$$U = \frac{1}{2} \left[\left(\frac{\partial \theta}{\partial \rho} \right)^2 - \frac{\sin^2 \theta}{\rho^2} \right], \quad V = \frac{1}{2} \cos^2 \theta,\tag{A.8}$$

depend only on the radial coordinate ρ . Furthermore the area A in Eq. (A.4) is taken to be a circle of radius R and the Cartesian components of the line-element vector $d\mathbf{s}$ are expressed in terms of the polar coordinates as $ds_1 = R \cos \phi d\phi$ and $ds_2 = R \sin \phi d\phi$. Relations (A.4) applied for $\mu, \nu = 1$ or 2 taken in all combinations reduce to the single virial relation

$$\int_0^R 2\pi \rho d\rho V(\rho) = \pi R^2 [V(R) - U(R)],\tag{A.9}$$

which must be satisfied for any radius R . Indeed, if we use the numerically calculated vortex profile $\theta = \theta(\rho)$ shown in Fig.3 to calculate the functions $U = U(\rho)$ and $V = V(\rho)$ from Eqs. (A.8), relation (A.9) is verified for all R . In particular, the limit $R \rightarrow \infty$ yields a nonvanishing contribution in the right-hand side thanks to the centrifugal term in the function U which leads to $U(R) \sim -1/2R^2$ because $\theta \rightarrow \frac{\pi}{2}$. The net result of this limit is

$$\int_0^\infty 2\pi \rho d\rho \cos^2 \theta = \pi,\tag{A.10}$$

which establishes the virial relation announced in Eq. (3.8). This relation no longer contradicts the existence of nontrivial vortex solutions but actually predicts analytically their anisotropy energy. However the exchange energy is (logarithmically) divergent thanks again to the centrifugal term.

REFERENCES

- [1] A.P. Malozemoff and J.C. Slonczewski, *Magnetic domain walls in bubble materials* (Wiley, New York, 1981).
- [2] V.G. Bar'yakhtar, M.V. Chetkin, B.A. Ivanov and S.N. Gadetskii, *Dynamics of topological magnetic solitons-experiment and theory* (Springer-Verlag, Berlin, 1994).
- [3] N. Papanicolaou, *Phys. Rev. B* **51**, 15062 (1995); and *Dynamics of domain walls in weak ferromagnets* (Crete preprint, 1996).
- [4] N.S. Manton, *Phys. Lett. B* **110**, 54 (1982); M. Atiyah and N. Hitchin, *The geometry and dynamics of magnetic monopoles* (Princeton University Press, Princeton, 1988); R.A. Leese, M. Peyrard and W.J. Zakrzewski, *Nonlinearity* **3**, 773 (1990).
- [5] N. Papanicolaou and T.N. Tomaras, *Nucl. Phys. B* **360**, 425 (1991).
- [6] S. Komineas and N. Papanicolaou, *Topology and dynamics in ferromagnetic media*, *Physica D* (in press).
- [7] G.H. Derrick, *J. Math. Phys.* **5**, 1252 (1964).
- [8] A.F. Andreev and V.I. Marchenko, *Sov. Phys. Uspekhi* **23**, 21 (1980).
- [9] B.A. Ivanov and A.K. Kolezhuk, *Phys. Rev. Lett.* **74**, 1859 (1995).
- [10] R.J. Donnelly, *Quantized vortices in helium II* (Cambridge University Press, Cambridge, 1991).
- [11] B.A. Ivanov, A.K. Kolezhuk and G.M. Wysin, *Phys. Rev. Lett.* **76**, 511 (1996).
- [12] A.A. Belavin and A.M. Polyakov, *JETP Lett.* **22**, 245 (1975).
- [13] N. Papanicolaou and W.J. Zakrzewski, *Physica D* **80**, 225 (1995); *Phys. Lett. A* **210**, 328 (1996).
- [14] R.S. Ward, *Phys. Lett. B* **158**, 424 (1985); W.J. Zakrzewski, *Nonlinearity* **4**, 429 (1991); R.A. Leese, *Nucl. Phys. B* **344**, 33 (1990).
- [15] P.J. Ruback, *Nucl. Phys. B* **296**, 669 (1988).
- [16] B.A. Ivanov and D.D. Sheka, *Phys. Rev. Lett.* **72**, 404 (1994).
- [17] A.A. Thiele, *Phys. Rev. Lett.* **30**, 230 (1973); *J. Appl. Phys.* **45**, 377 (1974).
- [18] N. Papanicolaou and T.N. Tomaras, *Phys. Lett. A* **179**, 33 (1993).
- [19] G. Stratopoulos and T.N. Tomaras, *Phys. Rev. B* **54**, 12493 (1996).
- [20] G.K. Batchelor, *An introduction to fluid dynamics* (Cambridge University Press, Cambridge, 1967).
- [21] A.R. Völkel, G.M. Wysin, A.R. Bishop and F.G. Mertens, *Phys. Rev. B* **44**, 10066 (1991).
- [22] A.R. Pereira and A.S.T. Pires, *Phys. Rev. B* **51**, 996 (1995).

FIGURE CAPTIONS

Figure 1: Illustration of the dimerization process for a finite portion of the square lattice cut along the diagonals. Solid and open circles denote the sites of the two intertwining sublattices.

Figure 2: Illustration of the tetramerization process of a finite portion of the square lattice.

Figure 3: The numerically calculated profile of a static vortex at weak anisotropy.

Figure 4: Spin vectors of a vortex and an antivortex projected on the (12) plane. Spins are shown at every fourth site of the original lattice and distances on the grid are measured according to Eq. (2.24) applied with $\varepsilon = 0.1$.

Figure 5: Three characteristic snapshots of a head-on collision of two like vortices originating at a relative distance $d = 5$ on the x -axis with initial velocities $\mathbf{v}_1 = (0.65, 0)$ and $\mathbf{v}_2 = (-0.65, 0)$. After collision the two vortices scatter at 90° and suffer an internal phase shift also equal to 90° . Vectors represent the projection of the field \mathbf{n} on the (12) plane.

Figure 6: Three characteristic snapshots of the annihilation process of a vortex and an antivortex that are initially at rest at a relative distance $d = 5$ on the x -axis. The vortex and the antivortex converge toward each other and are eventually annihilated into spinwaves. Vectors represent the projection of the field \mathbf{n} on the (12) plane.

Figure 7: Level contours of the energy density corresponding to the vortex-antivortex annihilation process shown in Fig. 6. After collision two distinct energy lumps emerge along the positive and negative y -axis but eventually dissipate into spinwaves.

Figure 8: Schematic illustration of the ground state in the presence of an external uniform magnetic field along the symmetry (third) axis. The canting angle δ is given by Eq. (5.3).

Figure 9: Time evolution of a pair of like vortices in the presence of a bias field $h = 1$. The two vortices are initially at rest, at a relative distance $d = 5$ on the x -axis, and subsequently orbit around each other instead of drifting away. Together with the initial configuration of the field \mathbf{n} projected on the (12) plane (upper entry) we provide snapshots at instances when the pair had rotated by 90° (middle entry) and 180° (lower entry). A 90° rotation in real space is always followed by a 90° internal phase shift.

Figure 10: Trajectories of the two rotating vortices of Fig. 9 obtained by tracking the points where $|n_3| = 1$. The two vortices originated at points A and B on the x -axis and the process was interrupted after the pair had completed a 180° rotation.

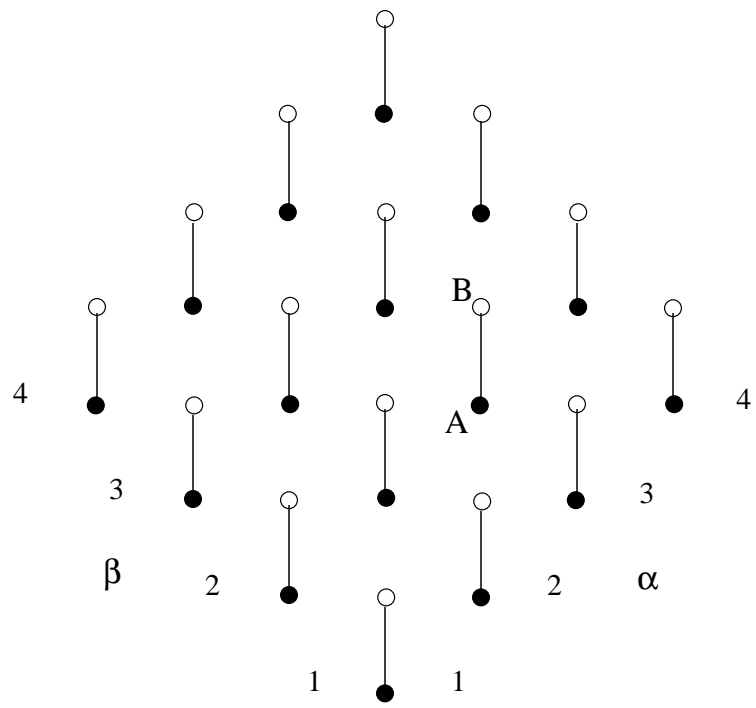
Figure 11: Evolution of the angular momentum of the vortex pair of Figs. 9 and 10 calculated from Eq. (5.54). The total angular momentum ℓ (solid line) is fairly

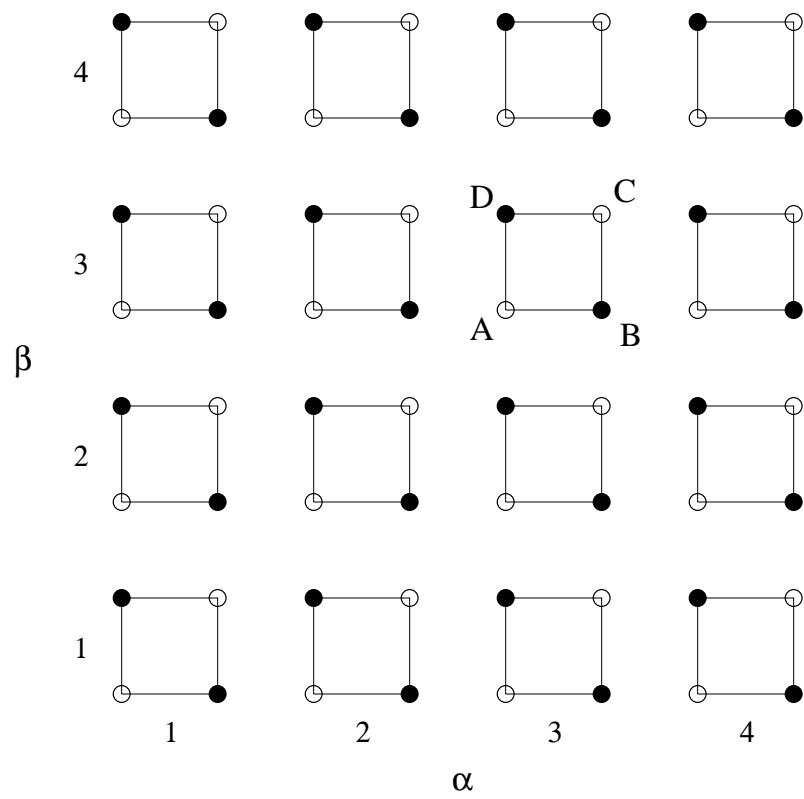
well conserved, except at late times when numerical instabilities develop on the finite lattice. The lower (upper) dashed line depicts the nontrivial time dependence of the first (second) term in Eq. (5.54).

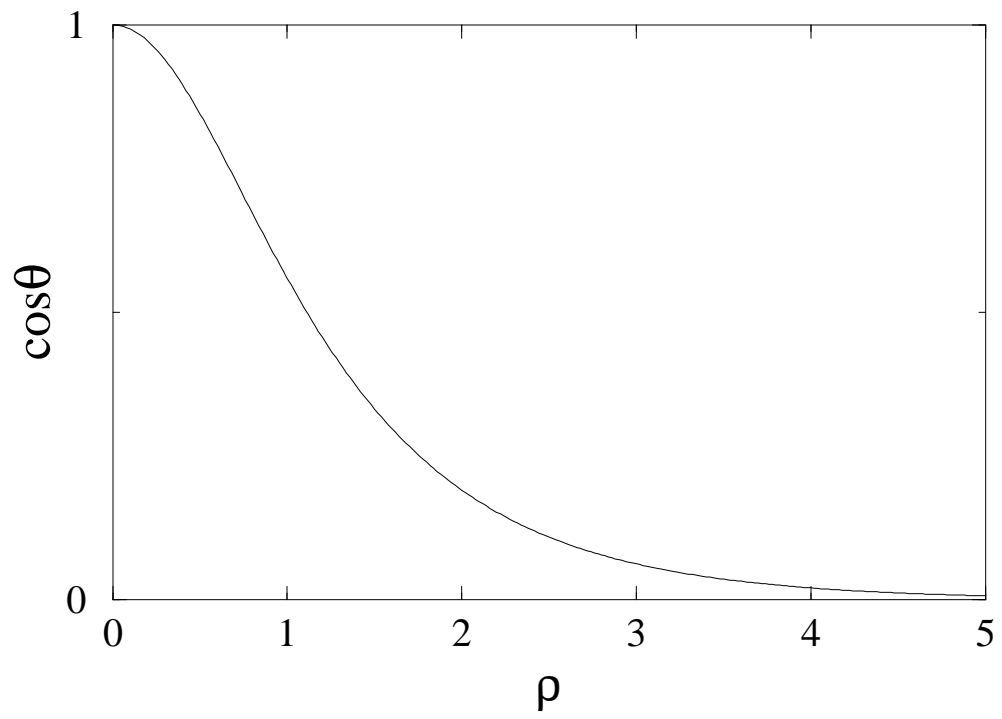
Figure 12: Evolution of a vortex-antivortex pair in the presence of a bias field $h = 1$. The vortex and the antivortex are initially at rest at the points $(2.4, -2.4)$ and $(-2.4, -2.4)$ of the xy -plane (upper entry). Instead of converging toward each other and annihilating, the pair moves in formation along the y -axis (Kelvin motion) as demonstrated by the snapshot of the lower entry taken at a later instance ($\tau \approx 20$).

Figure 13: Trajectories of the vortex and the antivortex of Fig. 12 originating at the points $B = (2.4, -2.4)$ and $A = (-2.4, -2.4)$. The actual trajectories (solid lines) were obtained by tracking the points where $|n_3| = 1$. The trajectories of the guiding centers (dashed lines) were calculated from Eq. (5.55) restricted to the corresponding half planes and are remarkably close to two parallel straight lines.

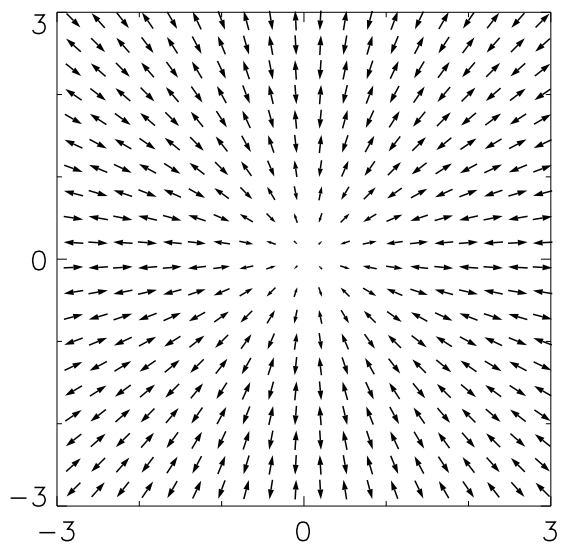
Figure 14: Evolution of the linear momentum of the vortex-antivortex pair of Figs. 12 and 13 calculated from Eq. (5.53). (We display only the y -component because the x -component vanishes.) The total linear momentum (solid line) is fairly well conserved, whereas the lower (upper) dashed line depicts the nontrivial time dependence of the first (second) term of Eq. (5.53).







vortex



antivortex

